AD-A018 856

HOVERCRAFT RIGID BODY RESPONSE TO FREE FIELD AIRBLAST

J. M. Ward

Naval Surface Weapons Center

Prepared for:

Defense Nuclear Agency

28 October 1975

NSWC/WOL/TR 75-42

NSWC/WOL/TR 75-42

NSWC

TECHNICAL REPORT

WHITE OAK LABORATORY

HOVERCRAFT RIGID BODY RESPONSE TO FREE FIELD AIRBLAST

By
J. M. Ward

28 October 1975

WHITE OAK LABORATORY
NAVAL SURFACE WEAPONS CENTER
WHITE OAK, SILVER SPRING, MARYLAND 20910

Approved for Public Release; Distribution Unlimited

NAVAL SURFACE WEAPONS CENTER
WHITE OAK, SILVER SPRING, MARYLAND 20910

UNCLASSIFIED
SECURITY CLASSIFICATION OF THIS PAGE (When Data Entered)

REPORT DOCUMENTATION PAGE		READ INSTRUCTIONS BEFORE COMPLETING FORM
1 REPORT NUMBER NSWC/WOL/TR 75-42	2 GOVT ACCESSION NO.	3 RECIPIENT'S CATALOG NUMBER
4 TITLE (and Subtitle) Hovercraft Rigid Body Response to Free Field Airblast		5 TYPE OF REPORT & PERIOD COVERED 6. PERFORMING ORG. REPORT NUMBER
7. AUTHOR(s) J. M. Ward		8. CONTRACT OR GRANT NUMBER(s)
9. PERFORMING ORGANIZATION NAME AND ADDRESS Naval Surface Weapons Center White Oak Laboratory White Oak, Silver Spring, Maryland 20910		10 PROGRAM ELEMENT, PROJECT, TASK AREA & WORK UNIT NUMBERS 62704H, ND013 ND01305 NDAND0130530124
11 CONTROLLING OFFICE NAME AND ADDRESS		12 REPORT DATE 28 October 1975 13 NUMBER OF PAGES
14 MONITORING AGENCY NAME & ADDRESS(if different from Controlling Office)		15 SECURITY CLASS. (of this report) Unclassified 15a. DECLASSIFICATION/DOWNGRADING SCHEDULE

16. DISTRIBUTION STATEMENT (of this Report)

Approved for public release; distribution unlimited

17. DISTRIBUTION STATEMENT (of the abstract entered in Block 20, if different from Report)

18 SUPPLEMENTARY NOTES

"This research was sponsored by the Defense Nuclear Agency under Subtask: V99QAXND013, Work Unit:NDAND0130530124, and Work Unit Title:Blast Tests on SES in transit."

19. KEY WORDS (Continue on reverse side if necessary and identify by block number)

Airblast	High Performance Ship	Blast Loading
Hovercraft	Rigid Body Response	Shock Waves
Air Cushion Vehicle (ACV)	Explosive Effects	
Surface Effect Ship (SES)	Blast Waves	

20. ABSTRACT (Continue on reverse side if necessary and identify by block number)

Vehicles in the class of surface effect ships (SES) and air cushion vehicles (ACV) respond to airblast loading in a manner different from that of conventional displacement-type ships. The SES/ACV class of vehicles has low hydrodynamic drag resistance to motion response and the air cushion chamber which levitates the vehicles can interact with the blast wave.

(continued)

DD FORM 1 JAN 73 1473 EDITION OF 1 NOV 65 IS OBSOLETE
S/N 0102-014-6601

UNCLASSIFIED
SECURITY CLASSIFICATION OF THIS PAGE (When Data Entered)

The rigid body response of a hovercraft (ACV) in an airblast environment was investigated by conducting free field HE explosive tests. The airblast loading was of short duration (25-35 msec free field positive phase). No significant vehicle rigid body response was observed for peak overpressures up to 4.0 psi; the vehicle response is shown to have been controlled by tether forces during airblast loading. Damage to the lift fan blades and the air cushion bag occurred at the 4.0 psi overpressure level.

Vehicle response was filmed and shipboard measurements of airblast pressures and accelerations were recorded. The experimental results are compared with calculations using a simple analytical model. The pressure and acceleration records contained local acceleration components produced by vehicle vibrational response to the loading. For this reason poor comparisons were obtained between data and calculations. Recommendations are suggested for future testing.

NSWC/WOL/TR 75-42 28 October 1975

HOVERCRAFT RIGID BODY RESPONSE TO FREE FIELD AIRBLAST

This report summarizes results and the analysis of the hovercraft/ airblast interaction tests performed at the Atlantic Fleet Weapons Range, U. S. Naval Station, Roosevelt Roads, Puerto Rico in June 1974.

The tests were part of a joint program which included airblast tests performed by the Naval Ship Research and Development Center (NSRDC) at the DASA Conical Shock Tube facility, Naval Surface Weapons Center, Dahlgren Laboratory. The shock tube results are reported separately by NSRDC.

The effort was funded by the Defense Nuclear Agency. The task was sponsored by Work Unit Number NDAND0130530124, Task Area Number ND01305.

The use of company names throughout this report is for technical information purposes only. No endorsement or criticism is intended.

J. W. Enig

J. W. ENIG
By direction

ACKNOWLEDGEMENTS

The author is indebted to Joseph Petes and Joseph F. Pittman for their advice on the test program and suggestions throughout the project.

The author is grateful to the laboratory personnel who participated in the field program: Phillip J. Peckham, Roy W. Huff, and William R. Shaffer. P. J. Peckham deserves special recognition for his assistance in planning and managing the field test program.

The author would like to thank Leonard Rudlin for his suggestions regarding the analytic approach and William W. Wassmann for his suggestions for handling the data.

The author wishes to acknowledge the able support for the field test operation from LCDR B. G. Cain and his staff at the Atlantic Fleet Weapons Range, Roosevelt Roads, Puerto Rico.

The author would also like to express appreciation for the cooperation received from Jim Ready and Roger Normandin at the Naval Ship Research and Development Center, Bethesda, Maryland in conducting the joint experimental/analytical program.

CONTENTS

		Page
1.	INTRODUCTION	5
	1.1 Background	5
	1.2 Scope of Investigation	5
	1.3 General Results	7
2.	EXPERIMENTAL PROGRAM	8
	2.1 Summary of Test Operation	8
	2.2 Test Site	8
	2.3 Field Layout	9
	2.4 Charge Construction	12
	2.5 Test Vehicle	12
	2.6 Instrumentation	15
	2.6.1 Airblast Measurements	15
	2.6.2 Acceleration Measurements	16
	2.6.3 Photography	16
	2.6.4 Data Recording System	16
3.	AIRBLAST RESPONSE MODEL	18
	3.1 Response Model	18
	3.2 Airblast Load Functions	20
	3.2.1 Front Face Load Function (Blast Side)	20
	3.2.2 Back Face Load Function (Lee Side)	25
4.	DISCUSSION OF RESULTS	27
	4.1 Free Field Airblast Measurements	29
	4.2 Shipboard Airblast Measurements and Calculated Load Functions	33
	4.3 Shipboard Acceleration Measurements and Calculated Vehicle Response	40
	4.4 Photographic Coverage	45
5.	SUMMARY OF RESULTS	46
6.	RECOMMENDATIONS	47
Appendix A:	Data Filter	A-1
Appendix B:	Integration of Acceleration Measurements	B-1
Appendix C:	Airblast Response of Model	C-1
Appendix D:	Airblast Response of Test Vehicle Determined from Acceleration Measurements	D-1
Appendix E:	Observations from Data Film HC14 for Shot 5	E-1

ILLUSTRATIONS

Figure	Title	Page
1	Field Layout	10
2	Test Vehicle Area	11
3	Charge-Booster-Detonator Arrangement	13
4	Test Vehicle Configuration	14
5	Model for Test Vehicle Showing Load Functions	19
6	Load Function Model	21
7	Free Field Airblast Results for Peak Overpressure and Positive Duration	24
8	Free Field Airblast Pressure History -- Shot 5, Channel 2	32
9	Shipboard Airblast Pressure Histories -- Shot 2, Channels 5-7	34
10	Shipboard Airblast Pressure Histories -- Shot 5, Channels 5-7	35
11	Shipboard Airblast Pressure Histories -- Shot 5, Channels 3, 4	36
12	Example of an Unfiltered Shipboard Airblast Pressure History -- Shot 3, Channel 6	37
13	Shipboard Acceleration Histories -- Shot 3, Channels 10, 12	41
14	Test Vehicle Response to Airblast Loading -- Horizontal Translation	43
15	Test Vehicle Response to Airblast Loading -- Lift	44
A-1	Unfiltered and Filtered Representations of Free Field Airblast Pressure History -- Shot 5, Channel 2	A-2
A-2	Transfer Function for 12th Order Low-Pass Butterworth Filter with a Half-Power Point at 2,000 Hz	A-3
D-1	Schematic of Test Vehicle Tether System	D-2

TABLES

Table	Title	Page
1	Airblast Load Function Parameters for the Overpressure Environments P_s^+ = 0.8, 2.0, and 4.0 psi.	22
2	Summary of Airblast and Acceleration Data.	28
3	Summary of Film Data	30
4	Free Field Airblast Record Characteristics for 1,000 Pound AN/FO Charges	31
5	Comparison between Calculated and Measured Values for Free Field Peak Overpressure and Peak Reflected Overpressure Experienced on Test Vehicle Blast Side	38

1. INTRODUCTION

1.1 Background

There is considerable interest in increasing the speed of the surface fleet; plans are to have an 80-knot capability in the not-to-distant future. For this reason, an effort is underway which includes research, development, and application of new surface ship (high performance ship) designs such as the surface effect ship (SES). Two 100-ton high speed test SES are in operation and a 2,000-ton vehicle design is in the advanced development stage. The SES differs from the conventional displacement-type ship. The SES is capable of being operated so that its weight is supported on a continuously generated cushion of air at pressures higher than ambient. The air cushion is maintained by fans and is contained beneath the vehicle structure by rigid sidewalls and flexible skirts at the bow and stern.

An area requiring study is the rigid body response of the SES in a nuclear blast environment. The interaction of such a long duration wave with the high speed SES can be expected to be different from that of a conventional surface ship with the same blast. The relatively high freeboard and small sidewall (hull) area below the water line accounts for some of this difference when considering the interaction of the positive phase of the blast wave with the SES; the vehicle experiences less hydrodynamic drag resistance to airblast loading than does a displacement ship. Also, interactions between the levitating pressure of the captured air bubble (air cushion) and the positive/negative phases of the airblast wave may contribute to significant SES response to loading not experienced by conventional craft.

1.2 Scope of Investigation

The field test project and analytical response model discussed in this report investigates some aspects of the rigid body response of SES to airblast loading. This project is part of a joint experimental/analytical program including the Naval Surface Weapons Center, White Oak Laboratory and the Naval Ship Research and Development Center. A hovercraft, an air cushion vehicle (which does not have rigid sidewalls to pierce the water surface as does the SES), was subjected to airblast loading and the resulting vehicle response was compared with calculations using a simple analytical model which was developed. Similar vehicles and the same motions computer code were used by both laboratories. The Naval Surface Weapons Center, White Oak Laboratory performed free field high explosive (HE) tests with the test vehicle whereas the Naval Ship Research and Development Center

conducted airblast tests at the DASACON Shock Tube Facility located at the Naval Surface Weapons Center, Dahlgren Laboratory. The free field tests subjected the test vehicle to overpressure/underpressure loading profiles of short duration, 25-35 msec free field positive phase duration. The shock tube tests subjected the test vehicle to long duration (∿250 msec) overpressure loading.*

A hovercraft was selected as the test vehicle because it was available commercially and could be easily modified for testing. There were no vehicles of the SES class available and construction costs for an SES test craft were too high. The test vehicle is not a scaled version of any specific military craft. However, this first study is only concerned with the response of an air cushion supported vehicle to an airblast overpressure environment. The test vehicle is one of the smaller operational hovercraft built and the explosive charge size used in the tests is the largest permitted at the test site location.

The free field tests were planned so as to subject the test craft to free field overpressure environments in the 1-5 psi range with the longest possible positive phase durations. This was performed to simulate as much as possible the interaction of a scaled version (larger size) of the test vehicle in a free field nuclear airblast environment. The only scaling parameter considered is the ratio of the positive duration of the overpressure loading to the airshock transit time across the vehicle.

For the test conditions (1,000 lb net explosive weight), the positive-duration/transit-time ratio for 4.0 psi overpressure (23.5 msec) is ∿ 6.75 for shock passage from starboard to port. Maintaining the same ratio, this would scale to a 9.3 KT charge with a positive duration of 625 msec (4.0 psi level) for a vehicle of the size of the 2000-ton SES. Considering a scale of the test vehicle to have the approximate dimensions of the 2,000-ton SES is only done for comparing results of the one scaling parameter discussed above. A more desirable "full-scale" positive duration is on the order of 2-3 seconds (megaton charge size) which was not possible for these tests.

Other test vehicle parameters which should be taken into consideration when modelling a vehicle such as the 2,000-ton SES for motion response tests are rigid sidewall construction, geometric similarity, center-of-gravity/center-of-pressure relative positions, mass, moments of inertia, and airblast-pressure/air-cushion-pressure ratio. To fine-tune the vehicle response model, the lift fan system and the cushion seal system responses should be scaled.

*The shock tube test results are discussed by READY.[1]

[1] READY, J., "Shock Tube Test Results on a Surface Effect Vehicle; Loading and Rigid Body Response," Naval Ship Research and Development Center Technical Note, to be published.

The scaling parameters can not all be satisfied simultaneously. For example, scaling the vehicle mass and the airblast-pressure/air-cushion-pressure ratio requires test vehicle weights of 200 lb (using a 2,000 ton full-size/model scale factor of S = 27 where mass is proportional to S^3) and 5000 lb (using full-scale plenum chamber pressure of ∿ 1 psi and test model area of 48" x 104"), respectively. The hovercraft weighed about 325 lbs for the tests described here. The vehicle was not modified for these tests to match specific scaling conditions.

Calculations such as those implied above were made to provide an estimate of the corresponding conditions for a "full-scale" craft. Predictions of the test vehicle response in airblast overpressure environments were computed very crudely by equating the change in vehicle momentum to applied airblast impulse loads. Vehicle motion response was calculated during data analysis using a 3-degree-of-freedom computer program for SES class of vehicles developed at the Naval Ship Research and Development Center.

Vehicle response on the order of several feet was expected under airblast loading test conditions. Shipboard instrumentation included airblast gages and accelerometers. The airblast environment was determined using free field airblast gages and technical photography was employed to record vehicle response to the airblast loading.

1.3 General Results

The main objective of this test program was to determined the rigid body response of a small (325 lb) air cushion vehicle to airblast loads from a series of free field small scale (1,000 lb net explosive weight) shots. The vehicle was to be subjected to blast loads while tethered in a hovering condition over water.

The main objective of the test was not accomplished; no significant vehicle rigid body response was obtained. The test vehicle response during airblast loading was controlled by tether forces which restricted motion. In the 4.0 psi overpressure environment, airblast impulse loads produced failures with the vehicle lift fan blades and air cushion bag. The fan blades sheared off and the air cushion bag ripped along the length of the craft on the lee side (from the blast).

Vehicle response during airblast loading was filmed and shipboard measurements of airblast pressures and accelerations were recorded. The experimental results are compared with calculations using a simple analytical model. The shipboard measurements of airblast pressures and accelerations contained local acceleration components produced by vehicle vibrational response to the loading. This resulted in poor comparison between the data and calculations.

Experience gained from the field test program provided several recommendations for future testing.

2. EXPERIMENTAL PROGRAM

2.1 Summary of Test Operation

A 325 pound hovercraft was subjected to airblast loads from 1,000 pound AN/FO charges. Test conditions included: 0.8, 2.0, and 4.0 psi positive overpressure levels. Data were acquired for five of six shots. The test vehicle presented a side profile (starboard) towards the blast for all five shots. (The thrust engine and bracket system were removed.)* The airblast test environments are listed below.

Shot Number 1 - 0.8 psi overpressure level
Non-hover mode** over water

Shot Number 2 - 0.8 psi overpressure level
Hover mode over water

Shot Number 3 - 2.0 psi overpressure level
Non-hover mode over water

Shot Number 4 - 2.0 psi overpressure level
Non-hover mode over shore

Shot Number 5 - 4.0 psi overpressure level
Hover mode over shore

The response of the test vehicle was filmed during airblast loading and shipboard measurements of accelerations and airblast pressures were recorded. Free field airblast pressure measurements were also made.

2.2 Test Site

The tests were conducted on the southeastern shore of Vieques Island, a part of the Atlantic Fleet Weapons Range (AFWR) which has headquarters at the U. S. Naval Station, Roosevelt Roads, Puerto Rico. The site designation is Area AIA R 7104, Range 3, and is operated by AFWR as a target range. The site is also maintained for explosive testing; charge sizes up to 1,000 pounds net explosive weight are permitted. The testing area is located near a body of water in which easy access between shore and water is available. The water surface is free from significant swell and wind waves for a large part of the time. Also, an unobstructed field of view is available for photographic coverage of the test and for observing the arming of the charges.

*The thrust engine was used as a substitute lift engine for shots 3, 4, and 5.

**Non-hover mode indicates lift engine is turned off. There is no air cushion.

2.3 Field Layout

The general field layout at the test site is shown in Figure 1. The test vehicle remained tethered in the same general vicinity for each test. Tests were conducted with the vehicle stationed over water and shore. Ground zero was moved between tests so as to provide the desired free field airblast pressure environments for the test vehicle. The instrumentation trailer, main generator, and transportainer were positioned so as to be no closer than approximately 1,100 feet from any ground zero location for protection of personnel and equipment from airblast and debris. During firings, members of the field team remained in the trailer or in the transportainer.

Figure 2 gives the field arrangement for the test vehicle. When the vehicle was positioned over water, the gage cables were secured to guideposts above the water. Enough slack was left in the cables so as not to hinder response of the test vehicle to airblast loads. A steel safety cable was bundled with the gage cables to prevent the test vehicle from moving much beyond the camera field of view after the airblast loading. The vehicle was tethered with marlin line to restrain vehicle translational motion induced by winds, water waves, or shore slope.*

Fiducial markers with a separation distance of 25 feet were positioned at the test vehicle location for use in determining vehicle translational motion during airblast response from film data. A mirror was located in the camera field of view for determining zero time of burst in the film data.

Ground zero was positioned approximately 50 to 100 feet inland with the charge at a height of burst of six feet. Using burst height reduced cratering and prevented any significant environmental and ecological damage to the test area.

*The original tethering system included bundled strands of ten pound test fishing line placed in series with the marlin line. This tethering system would fail during test preparation from wind gust loads and had to be replaced with a complete marlin line tethering system. However, the complete marlin line tethering system did not release the test vehicle as planned during airblast loading. The marlin line proved to be too strong for the loads encountered.

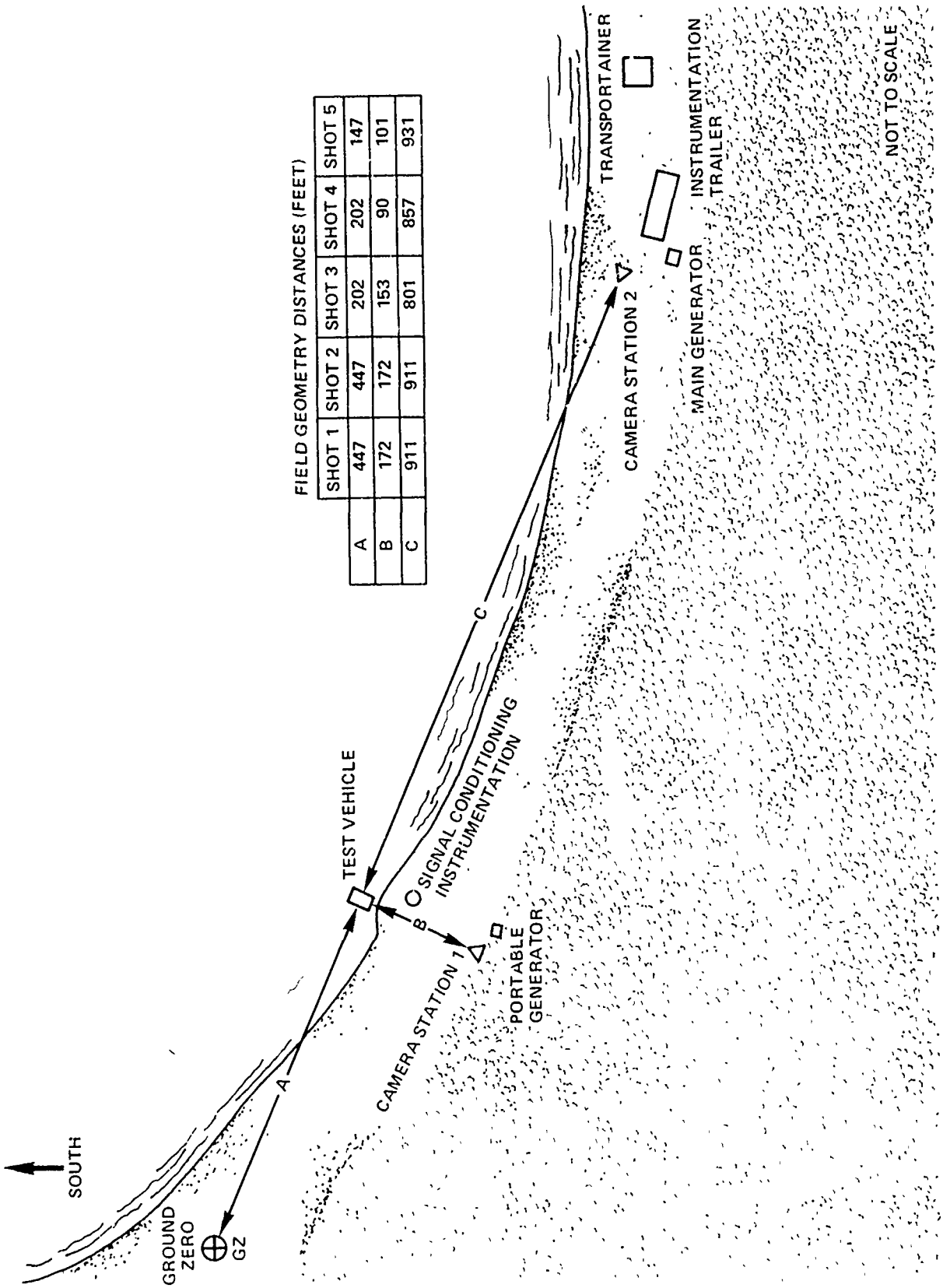

FIELD GEOMETRY DISTANCES (FEET)

	SHOT 1	SHOT 2	SHOT 3	SHOT 4	SHOT 5
A	447	447	202	202	147
B	172	172	153	90	101
C	911	911	801	857	931

FIG. 1 FIELD LAYOUT

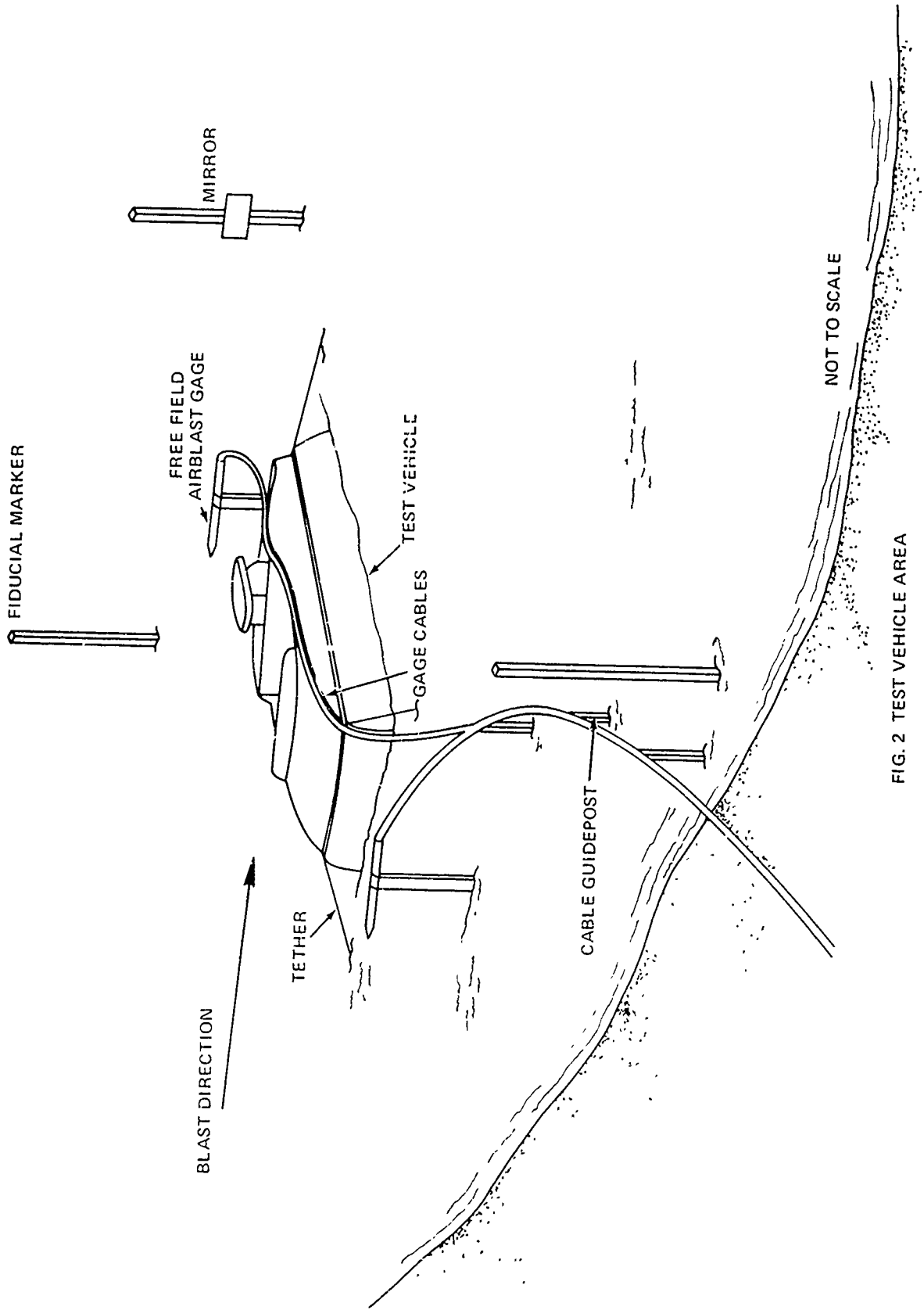

FIG. 2 TEST VEHICLE AREA

2.4 Charge Construction

All charges were right circular cylinders. The explosive material, premixed AN/FO*, was poured into a three foot diameter container mounted on a platform four and one-half feet high.

The booster, five pounds of composition C-4, was placed on the platform at the center of the base of the cylinder. The 1,000 pound charge was then poured into the cylinder reaching a height of 30 inches. To initiate, an engineer special detonator was placed in the booster from below the platform through a pre-drilled hole. The charge arrangement is shown in Figure 3.

2.5 Test Vehicle

The test vehicle is a Hoverbug manufactured by Eglen Hovercraft, Inc. of Terre Haute, Indiana. The craft in test configuration is shown in Figure 4. The vehicle is a two-passenger open cockpit recreational hovercraft (air cushion vehicle (ACV)).

The air cushion is maintained by a two foot diameter ten-bladed fan powered by a 22 horsepower two-cycle engine mounted just aft of the open cockpit. Thrust is provided by a 25 horsepower two-cycle engine which drives a three foot diameter, two-bladed propeller. The air cushion skirt is a bag type fabricated with neoprene-coated nylon. The hull is constructed of Cycolacbrand ABS which is a high gloss, high impact plastic.

Vehicle dimensions are

Length, cushion on	-	10 feet
Beam, cushion on	-	6.5 feet
Draft, afloat	-	0.5 feet
Skirt depth	-	1 foot

Vehicle weight in test configuration was 325 pounds. The vehicle as received from the factory was modified. The thrust engine was removed and used as a spare lift engine and several additional sections of the craft were removed so as to clean up the vehicle profile (as a blast target) and to facilitate mounting instrumentation. The

*AN/FO refers to a mixture of ammonium nitrate and fuel oil proportioned 94.5/5.5 ± 0.1% by weight. Bulk density is 0.85 to 0.90 grams/cc with a particle size distribution being at least 90% + 14 mesh. The fuel oil is No. 2 diesel colored with red dye for use in indicating the presence of the fuel oil in the AN/FO mixture. The mixture designated Standard Product NCN 1 was prepared by Gulf Oil Company for these tests. Additional information on AN/FO properties is given by SADWIN and SWISDAK.[2]

[2]SADWIN, L. D. and SWISDAK, M. M., Jr., "Blast Characteristics of 20 and 100 Ton Hemispherical AN/FO Charges, NOL Data Report," Naval Ordnance Laboratory Report NOLTR 70-32, Mar 1970.

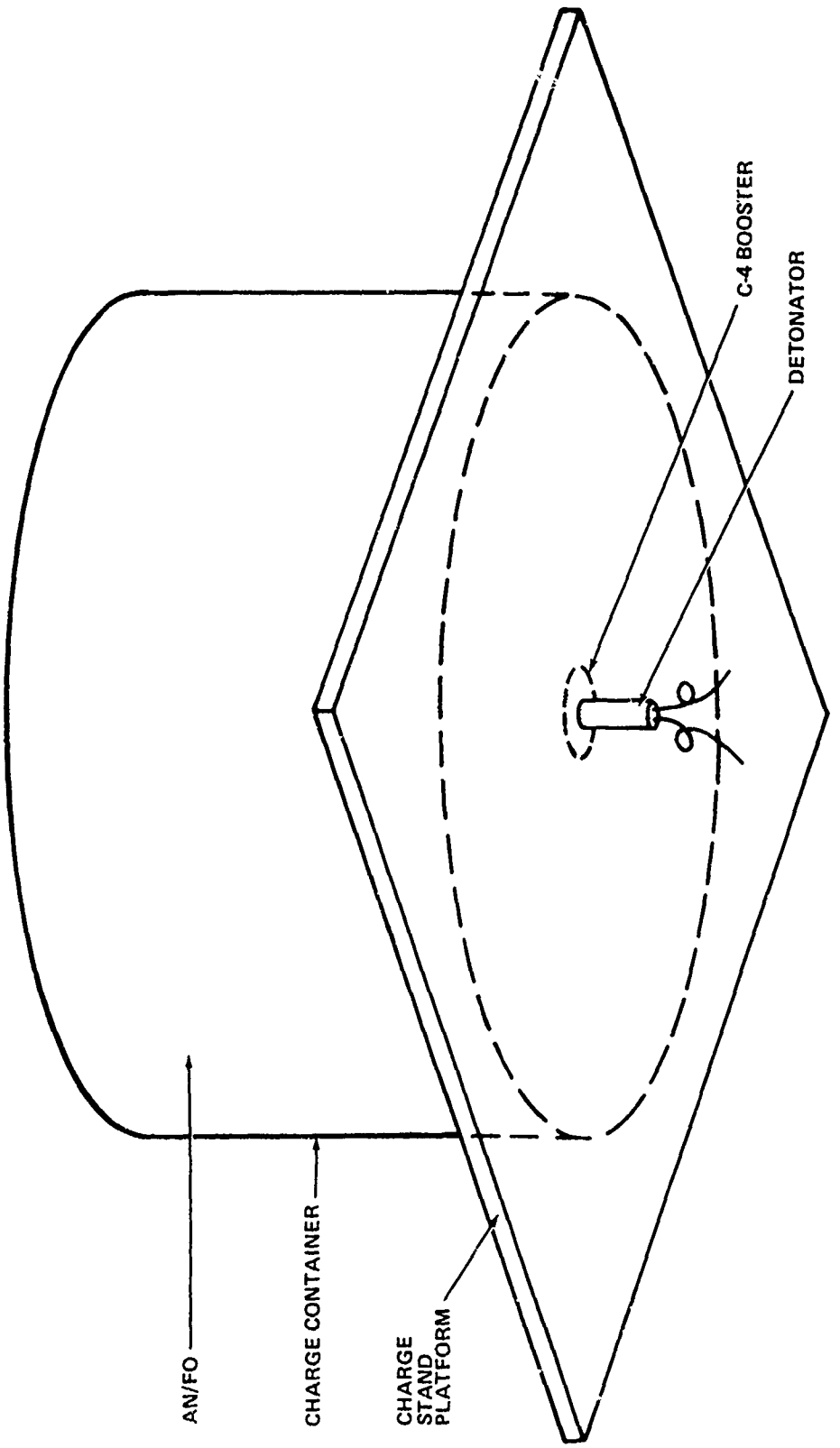

FIG. 3 CHARGE-BOOSTER-DETONATOR ARRANGEMENT.

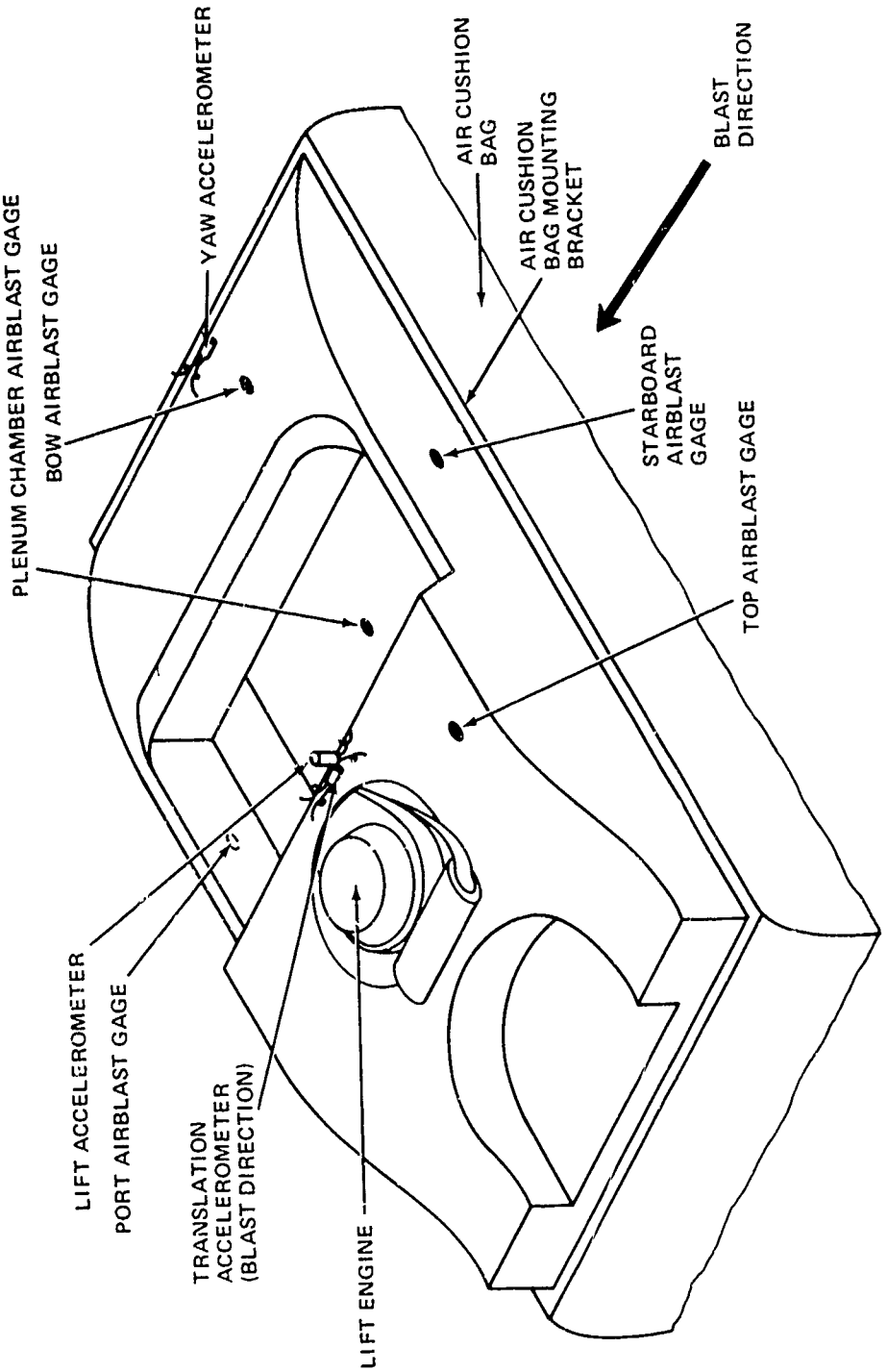

FIG. 4 TEST VEHICLE CONFIGURATION

removed sections include: seat, wind-screen, battery, rudders, thrust engine with bracket assembly, muffler, and steering wheel.

The Hoverbug was selected as the test vehicle for the following reasons:

(1) The craft is an operational vehicle possessing an air cushion lift system which is the distinguishing difference between the SES/ACV and the conventional displacement-type craft.

(2) The vehicle is small enough (maximum dimension is 10 feet) to be mounted in the DASACON shock tube facility at the Naval Surface Weapons Center, Dahlgren Laboratory for airblast tests conducted by the Naval Ship Research and Development Center.

(3) The craft (ACV) is readily available commercially. There was no vehicle of the SES class available.

The Hoverbug is not a scaled version of any existing military craft, but this is no serious drawback, since in this preliminary study only the interaction of an air cushion supported test vehicle to airblast loading is being investigated.

2.6 Instrumentation

2.6.1 Airblast Measurements. Free field airblast pressure measurements were made with Celesco LC-33 pencil-type blast pressure gages. The normal charge output of these piezoelectric gages was converted to voltage output using type 402A13 source followers made by PCB Piezotronics, Inc. Gage signals were recorded on magnetic tape. Two free field airblast measurements were taken for each shot; one gage each off the bow and stern of the test vehicle at a total gage separation distance of 15 feet. The gages were each positioned on the order of two feet above either the water or shore surface.

Celesco type LC-70 pressure transducers were used to measure shipboard airblast pressure-time histories. Shipboard airblast gage locations are indicated in Figure 4 and listed below.*

Bow airblast gage - Located 11 inches aft of bow and 11 inches in from starboard side.

Plenum chamber airblast gage - Located 42 inches aft along longitudinal center line from bow. The gage was mounted in the deck floor.

Top airblast gage - Located 15-1/2 inches aft of passenger well (52 inches aft of bow) and 6 inches in from starboard side. The gage was 12 inches from lift engine duct.

*Dimensions refer to the plastic hull structure. The width of the air cushion bag with cushion on is not included.

Starboard and Port airblast gages - Centered vertically on side panel 4-1/2 inches above air cushion bag bracket and 49 inches aft of bow.

The plastic hull was drilled and tapped for mounting the gage directly. No additional mass or stiffening members were added to the structure. The normal charge output of the gages was converted to voltage output and amplified using Kistler 503 or 504 charge amplifiers. Gage signals were recorded on magnetic tape.

2.6.2 Acceleration Measurements. Vehicle accelerations were measured with accelerometers mounted on the test vehicle. Shipboard accelerometer locations are indicated in Figure 4 and listed below.*

Yaw accelerometer - Located 4-1/2 inches aft of bow along longitudinal center line.

Translation and Lift accelerometers - Located 52 inches aft of bow along longitudinal center line and 23 inches above deck floor. This position is 3 inches forward and 7 inches above approximate vehicle center-of-gravity location.

The accelerometers were mounted on aluminum angle stock which was used for strengthening the structure at the gage locations. Three acceleration components were measured; lift (heave), rotation (yaw), and horizontal translation (sway - in direction of blast). The accelerometers were types 2262-25 piezoresistive low "g" gage made by Endevco (for the lift gate) and CEC Model 4-202-0001 ±100g (for the yaw and translation gages). The transducer signals were amplified by Ectron 750EK differential D.C. amplifiers and recorded on magnetic tape.

2.6.3 Photography. Technical photographic coverage of the test-vehicle/airblast interaction was acquired using one 16mm Hycam and three 16mm Photosonic cameras. Camera speeds used were 400 and 1,000 fps with timing pulses provided at 100 Hz or 1,000 Hz. The camera station locations are indicated in Figure 1. Camera station 1 was located near the test vehicle, within 90-175 feet with cameras directed towards the bow of test vehicle. Cameras of station 2 were oriented towards the port side of the test vehicle with a vehicle/station separation distance of 800-950 feet.

2.6.4 Data Recording System. The data were recorded on a CEC type VR3300 14-channel tape recorder, FM mode. One channel was set up for timing, IRIG A time code, and one channel for voice track which also recorded the firing pulse. There were seven channels for airblast gages (two free field and five shipboard gages) and five channels

*Dimensions refer to the plastic hull structure. The width of the air cushion bag with cushion on is not included.

for shipboard accelerometers (two of these channels were redundant with different set-up voltages).

3. AIRBLAST RESPONSE MODEL

3.1 Response Model

Calculations of the test vehicle rigid body response to airblast loads were obtained using computer code TRANS* which is a three-degree-of-freedom motions program developed for computing surface effect ship (SES) response to airblast loads. Vehicle model geometry and general load functions are shown in Figure 5. Note that the model dimensions used in the calculations differ from the vehicle cushion-on dimensions listed in Section 2.5 Test Vehicle of the text. The cushion-on dimensions include the air cushion bag width, which the model dimensions do not include.

The model represents the test vehicle as a box-like structure. Airblast loads are imposed only on the blast and lee sides of the model. Vertical loads produced by passage of the airshock above and below the model are not considered. Vehicle model accelerations in the vertical direction are not considered in this analysis even though they are quite important in determining the total motion response. This is because effects such as vehicle/surface and shock/air-cushion interactions are excluded in order to simplify these first calculations. The horizontal forces are applied at the center of pressure (C.P.) shown in Figure 5. Transferring the forces to the center of gravity (C.G.) location gives a moment about the Z-axis and a net horizontal force in the X-direction.** Resultant velocities and translations (linear and rotational) are then calculated using vehicle accelerations produced by the imposed loads.

Program TRANS was written for an SES; however, the test vehicle was an ACV. Both types of vehicles are supported by an air cushion, a continuously pressurized chamber beneath the vehicle, but the SES has rigid starboard- and port-sidewalls which are partially submerged in water during cushion-on operation. Hydrodynamic forces included in program TRANS to account for the sidewall/water interaction are deleted in the present calculations. No restraint of vehicle response to the airblast loads such as friction or vehicle interference with the water surface is considered in this simple analysis.

*TRANS was written at the Naval Ship Research and Development Center (NSRDC), Bethesda, Maryland where the code is undergoing continuing development and documentation under the name SESRGD.

**The C.P. location is the centroid of the composite area formed by the area LxD shown in Figure 5 and the cross-sectional area of the lift engine (not shown in the figure) which projects above the vehicle structure. The C.G. location is determined from the relative locations of the vehicle weight distributed between the lift engine and the plastic hull structure. Additional weight concentrations within the test vehicle are not considered.

MASS = 0.841 LB SEC^2 IN^{-1}

$(I_Z)_{CG}$ MOMENT OF INERTIA = 161.6 LB IN SEC^2

OVERALL MODEL DIMENSIONS (INCHES)

W	=	48
D	=	18
L	=	104

CENTER OF GRAVITY LOCATION (INCHES)

XCG	=	24.0
YCG	=	10.9
ZCG	=	55.0

CENTER OF PRESSURE LOCATIONS (INCHES)

YCP	=	9.8
ZCP	=	52.0

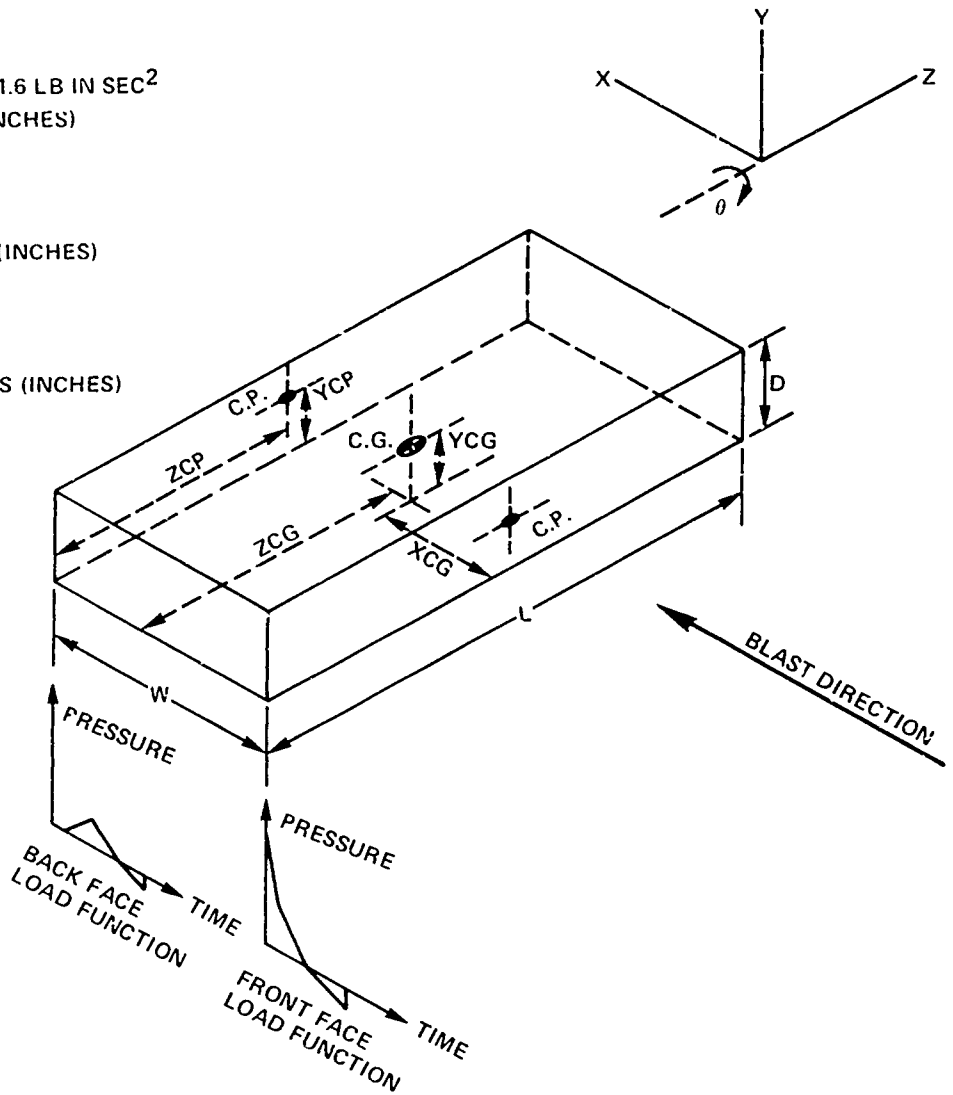

FIG. 5 MODEL FOR TEST VEHICLE SHOWING LOAD FUNCTIONS

3.2 Airblast Load Functions

The airblast load functions* corresponding to the three test environments are defined in Figure 6. All pressure-time profiles are fitted by straight lines; each exponential pressure decay profile formulation presented by BRODE[3] can be well represented by a straight line segment for these airblast conditions.

The coordinates for the load functions given in Figure 6 are determined as shown on the following pages.** Airblast parameters used in the load function definitions for the three test environments are listed in Table 1. Note that the dynamic pressure (q_s) contribution is not included in two test environment calculations (P_s^+ = 0.8, and 2.0 psi). The dynamic pressure is negligible in comparison with the static overpressure/underpressure levels for these two cases.

3.2.1 Front Face Load Function (Blast Side)

$t_1 = 0$, airblast arrival time at front surface (blast side) of vehicle

$P_1 = 2\left(\frac{7P_0+4P_s^+}{7P_0+P_s^+}\right)P_s^+$, peak reflected overpressure

P_0 is the ambient pressure and P_s^+ is the peak overpressure.

$t_2 = \frac{3D}{U}$, clearing time for front surface

$P_2 = P^+(\tau_2) + C_{df}\, q(\omega_2)$, stagnation overpressure at onset of drag phase

where $P^+(\tau) = P_s^+(ae^{-\alpha\tau} + be^{-\beta\tau} + ce^{-\gamma\tau})\ (1-\tau)$

$q(\omega) = q_s(1-\omega)^2\ (de^{-\delta\omega} + fe^{-\phi\omega})$

*The force functions are obtained by multiplying the airblast pressure functions by the side profile surface area of the vehicle. The area in this case is 1940 square inches.

**Unless otherwise specified, defining equations are taken from BRODE[3] which are also reproduced in a more recent report by KAPLAN, LEWIS, and MORRIS.[4]

[3]BRODE, H. L., "A Review of Nuclear Explosion Phenomena Pertinent to Protective Construction", Report R-425-PR, The Rand Corporation, Santa Monica, California, May 1964.

[4]KAPLAN, K., LEWIS, K. S., and MORRIS, P. J., "Blast Loading and Response of Military Equipment", BRL Contract Report No. 178, prepared by URS Research Company, San Mateo, California for USA Ballistic Research Laboratories, August 1974.

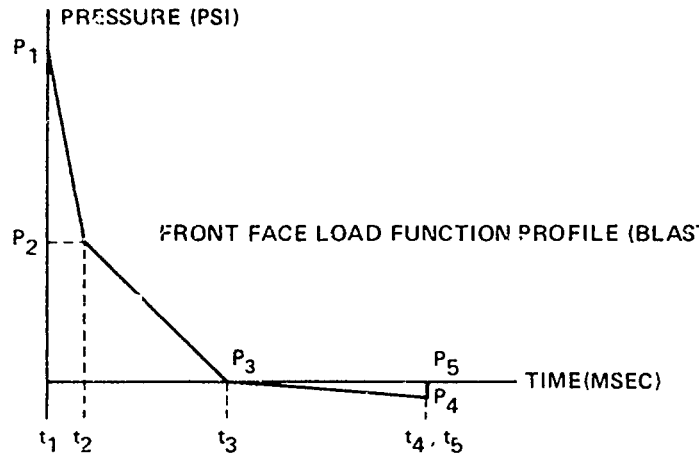

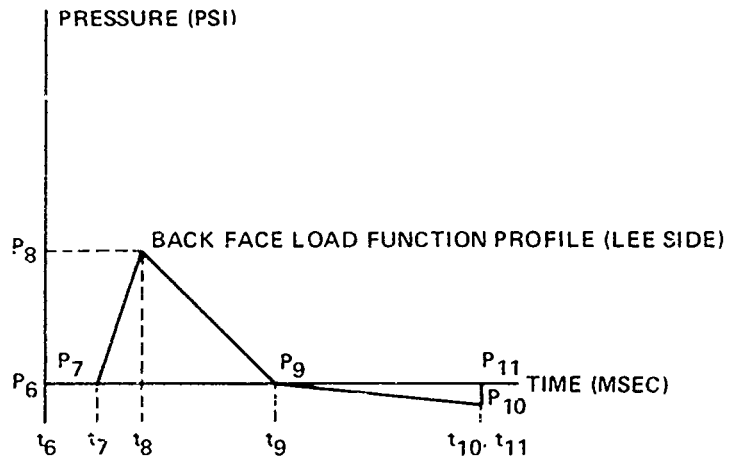

LOAD FUNCTION PROFILE COORDINATES FOR THREE AIRBLAST OVERPRESSURE ENVIRONMENTS

	P_s^+ = 0.8 PSI		P_s^+ = 2.0 PSI		P_s^+ = 4.0 PSI	
	t (MSEC)	P (PSI)	t (MSEC)	P (PSI)	t (MSEC)	P (PSI)
1	0	1.64	0	4.23	0	8.90
2	3.8	0.70	3.8	1.66	3.6	3.26
3	34.5	0	27.5	0	23.5	0
4	75.9	-0.28	60.5	-0.70	51.6	-1.40
5	75.91	0	60.51	0	51.61	0
6	0	0	0	0	0	0
7	3.3	0	3.3	0	3.2	0
8	6.8	0.62	6.8	1.39	6.7	2.38
9	37.8	0	30.8	0	26.7	0
10	79.2	-0.28	63.8	-0.70	54.8	-1.4
11	79.21	0	63.81	0	54.81	0

FIG. 6 LOAD FUNCTION MODEL

Table 1

AIRBLAST LOAD FUNCTION PARAMETERS
FOR THE OVERPRESSURE ENVIRONMENTS P_s^+ = 0.8, 2.0, AND 4.0 PSI

Airblast Parameters*	P_s^+ = 0.8 psi	P_s^+ = 2.0 psi	P_s^+ = 4.0 psi
q_s (psi)	-	-	0.37
a	0.94	0.89	0.86
b	0.065	0.11	0.14
c	0	0	0
d	0	0	0.88
f	0	0	0.12
α	0.10	0.25	0.50
β	0.023	0.033	0.042
γ	0	0	0
δ	0	0	1.15
ϕ	0	0	12.7

NOTES:

*Airblast parameters are used in Section 2.3.1 Front Face Load Function (Blast Side) in the expression defining overpressure. The parameters are taken from reference 3.

The clearing time represents the end of the diffraction phase and the beginning of the drag phase. Interactions between the shock wave and rarefaction waves are now negligible and the surface is loaded as if subjected to steady flow. D is the vehicle height (the smaller characteristic frontal dimension) and is defined in Figure 5. U is the shock propagation velocity.* C_{df} is the drag coefficient for the front surface and is equal to $C_{df} = 0.8$ (KAPLAN, LEWIS, and MORRIS[4]). q_s is the peak dynamic pressure given by BRODE[3] as a function of peak overpressure. $\tau = \frac{t}{t_p^+}$ and $\omega = \frac{t}{t_v^+}$ with t_p^+ and t_v^+ representing the overpressure duration and the positive velocity duration (the dynamic pressure duration), respectively. For these airblast conditions $t_v^+ \cong t_p^+$ which means that $\omega \cong \tau$. P_2 is evaluated for $\tau = \tau_2 = \frac{t_2}{t_p^+}$.

The constants a, b, c, d, f, α, β, γ, δ, and ϕ are presented by BRODE[3] as functions of peak overpressure. (See Table 1 for specific values used.)

$t_3 = t_p^+$, overpressure duration (positive phase)

$P_3 = 0$, ambient overpressure

Values for t_p^+ are taken from AN/FO airblast data (SADWIN and PITTMAN[5]) displayed in Figure 7.

$t_4 = t_p^+ + t_p^-$, sum of overpressure and underpressure durations

$P_4 = P^-$, final underpressure value before arrival of second shock

The underpressure duration (negative phase) is approximated as $t_p^- \cong 1.2\ t_p^+$ which is determined by the arrival of the second shock in the present experimental free-field airblast data.

The final underpressure value** before arrival of the second shock is approximated as $P^- = 0.35\ P_s^+$. This relation is determined

*The shock propagation velocity is determined from the present time-of-arrival data for the starboard and port airblast gages. The value is U = 1150 ft/sec which is used for all calculations.

**The approximation is very crude. There are only five sets of data and a single estimate is made for all test environments.

[5]SADWIN, L. D. and PITTMAN, J. F., "Airblast Characteristics of AN/FO, Phase 1," Naval Ordnance Laboratory Report NOLTR 69-82, Apr 1969.

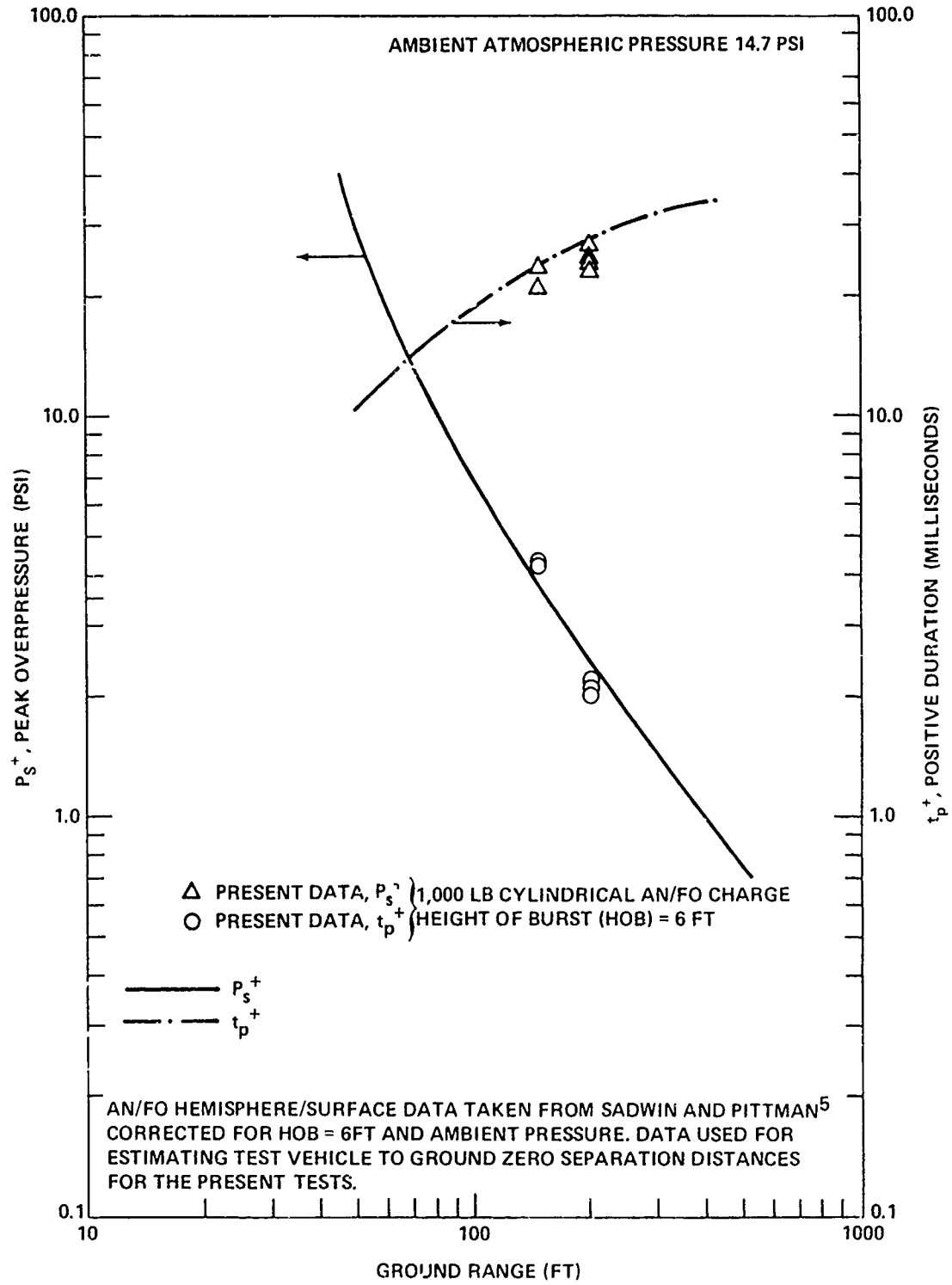

FIG. 7 FREE FIELD AIRBLAST RESULTS FOR PEAK OVERPRESSURE AND POSITIVE DURATION

from the present experimental free field airblast data. A straight line segment is used for the load profile between coordinates (t_3, P_3) and (t_4, P_4).

$t_5 = t_4 + \Delta t$, load function cut-off time on front face

$P_5 = 0$, ambient overpressure

A finite slope is defined for computational purposes with Δt = 0.01 msec.

3.2.2 Back Face Load Function (Lee Side)

$t_6 = t_1 = 0$, airblast arrival time at front surface of vehicle

$P_6 = 0$, ambient overpressure

$t_7 = \frac{W}{U}$, airblast transit time across vehicle

$P_7 = 0$, ambient overpressure

The vehicle beam dimension (W) is defined in Figure 5.

$t_8 = t_7 + t_*$, termination of clearing time for rear surface

$P_8 = P^+(\tau_*) + C_{db}\, q(\tau_*)$, stagnation overpressure at onset of drag phase

The rear surface clearing time (t_*)as given by KAPLAN, LEWIS, and MORRIS[4] is

$$t_* = (2.7 + 0.77 \frac{P_s^+}{P_0}) (\frac{D}{U}) .$$

where $\tau_* = \frac{t_*}{t_p^+}$ and C_{db} is the drag coefficient for the rear surface which is equal to $C_{db} = -0.3$ (KAPLAN, LEWIS, and MORRIS[4]).

$t_9 = t_7 + t_p^+$, termination of overpressure on rear surface

$P_9 = 0$, ambient overpressure

$t_{10} = t_9 + t_p^-$, termination of underpressure on rear surface

$P_{10} = P^-$, final underpressure value before arrival of second shock

$t_{11} = t_{10} + \Delta t$, load function cut-off time on rear surface

$P_{11} = 0$, ambient overpressure

4. DISCUSSION OF RESULTS

Free field airblast, shipboard airblast, and shipboard acceleration measurements acquired in the present tests are listed in Table 2. Table notations provide brief descriptions of data. The gages and their locations are given in Section 2.6 Instrumentation.

The original data were converted from analog to digital format. The computer code MRWSRD* was used to perform digital filtering and to provide graphical display of data. The choice of digital filter used and the modification to the data is discussed briefly in Appendix A. A check into the data reduction procedure revealed that improper low-pass filter and pulse-generator plug-in units were used with the tape recorder for data playback. A comparison made between the original analog data as displayed by Visicorder output and the digital data represented in graphical form by MRWSRD provides the following results: Graphical measurements of characteristic wave-form durations agree within 10% and wave-form amplitudes agree within 20%. The digital amplitude values are low with respect to the analog values. This variation between the analog and digital data records for these tests is not significant enough, considering the quality of the original data, to warrent repeating the data reduction procedure.

Only selected airblast and acceleration records are included in this report. The records to be discussed in subsequent sections of this report are listed below.

Free Field Airblast - Stern (Channel 2) - Shot 5

Shipboard Airblast - Bow (Channel 3) - Shot 5

- Top (Channel 4) - Shot 5

- Port (Channel 5) - Shot 2, Shot 5

- Starboard (Channel 6) - Shot 2, Shot 5

- Plenum (Channel 7) - Shot 2, Shot 5

*The name MRWSRD (MR WISARD) is an acronym for Multi-Record Wave Investigator for Sine and Random Data. Code description including options and input instructions are given by REED.[6]

[6]REED, R. S., "A Digital Computer Program for the Analysis of Wave-Form Data," Naval Ordnance Laboratory Report NOLTR 69-28, January 1969

Table 2

SUMMARY OF AIRBLAST AND ACCELERATION DATA

Channel	Gage Designation	Shot 1	Shot 2	Shot 3	Shot 4	Shot 5
	Free Field Airblast					
1	Bow	*	*	***	B	A
2	Stern	*	*	B	B	A
	Shipboard Airblast					
3	Bow	B,D	**	B,D	B,D	D
4	Top	**	**	B,D	B,D	D
5	Port	A	A	A	A	C
6	Starboard	B	C	B	B	D
7	Plenum	**	**	D	B,D	D
	Shipboard Acceleration					
8	Yaw	**	*	*	*	*
9	Translation	**	*	A	E	E
10	Lift	**	*	A	E	**
11	Yaw	**	*	*	*	*
12	Translation	**	*	A	E	E

NOTES:
A - Signal is recorded.
B - Recorded signal contains appreciable noise. See Figure 12 for example.
C - Recorded signal contains appreciable post shock noise. See Figure 10(b) for example.
D - Recorded signal contains post-shock signal drift. See Figure 10(a) for example.
E - Recorded signal is clipped.
*No signal is recorded.
**Data is not discernable from high signal noise.
***Calibration step contains noise. No calibrated data.

Shipboard Acceleration - Lift (Channel 10) - Shot 3

- Translation (Channel 12) - Shot 3

The data listed above include a free field airblast record, at least one record for each shipboard airblast gage location*, and one record each for the lift and translation accelerometers. No yaw acceleration data were obtained.** The quality of the airblast and acceleration data acquired in these preliminary tests is poor. For this reason, only a qualitative analysis of the results is given in the main text of this report. More detailed analyses are contained in appendices.

A listing of the data films of the text-vehicle/airblast interaction for the five shots in the testing program are provided in Table 3. Descriptive information on 16 films is included in the table. The quality of the film data is excellent. However, there was no significant test vehicle rigid body response to the airblast loading to analyze. A summary of the response observed is contained in the main text of this report with more detailed comments provided in an appendix.

4.1 Free Field Airblast Measurements

Free field airblast data were not received for Shots 1 and 2. Following Shot 2 the source followers for the free field airblast gages were replaced and data were obtained for Shots 3, 4 and 5. These results, free field airblast peak overpressure levels and positive durations, are compared in Figure 7 with earlier AN/FO airblast data.***

Peak overpressure and underpressure values are listed in Table 4 along with positive and negative phase durations for all free field airblast data acquired during these tests. A free field airblast record is displayed in Figure 8. Note the appearance of a second shock in the record. The negative phase ends upon arrival of the second shock in the load function formulation.

There is a portion of the negative phase which follows the second shock in Figure 8 that is not included in the load function model. For the example shown in the figure the total elapsed time between shock arrival (arrow a) and final return to ambient pressure

*Port, starboard, and plenum records are included for both hovering test configurations, Shot 2 and Shot 5.

**Replacements were not available during the test for this accelerometer which malfunctioned. Plans were to calculate yaw accelerations from the couple resolved between accelerometers positioned at the "yaw" and "translation" locations shown in Figure 4.

***Figure 7 should contain four side-on overpressure data points at the 200 foot ground range location instead of just three. One record with a noisy calibration step is deleted.

Table 3

SUMMARY OF FILM DATA

Film Designation	Shot Number	Test Environment*	Camera Station	Camera (Film)**	Frames Per Second	Camera Lens (mm)
---***	1	0.8-NW	1	PH	--	25
--	1	0.8-NW	1	PH	--	50
HC1	1	0.8-NW	2	PH(C)	400	150
HC2	1	0.8-NW	2	HY(C)	1000	150
HC3	2	0.8-HW	1	PH(C)	400	25
HC4	2	0.8-HW	1	PH(B&W)	1000	50
HC5	2	0.8-HW	2	PH(B&W)	400	150
HC6	2	0.8-HW	2	HY(C)	1000	150
--	3	2.0-NW	1	PH(C)	--	25
HC7	3	2.0-NW	1	PH(C)	1000	50
HC8	3	2.0-NW	2	PH(C)	400	150
HC9	3	2.0-NW	2	HY(C)	1000	150
HC10	4	2.0-NS	1	PH(B&W)	400	25
HC11	4	2.0-NS	1	PH(C)	1000	50
--	4	2.0-NS	2	PH	--	150
HC12	4	2.0-NS	2	HY(C)	1000	150
HC13	5	4.0-HS	1	PH(C)	400	25
HC14	5	4.0-HS	1	PH(C)	1000	50
HC15	5	4.0-HS	2	PH(C)	400	150
HC16	5	4.0-HS	2	HY(C)	1000	150

NOTES:
*Test environment notation. The number gives the airblast overpressure environment in units of psi. The abbreviations represent - N(non-hover), H(hover), W(water), and S(shore). For example: 0.8-NW -- 0.8 psi overpressure environment with test vehicle in non-hover mode over water.
**Camera (film) notation. PH - Photosonic camera, HY - Hycam camera, (C) - color film, (B&W) - black and white film.
***Blank table entry indicates no film data acquired.

Table 4

FREE FIELD AIRBLAST RECORD CHARACTERISTICS
FOR 1,000 POUND TN/FO CHARGES

Shot Number	Data Channel	Distance to Ground Zero (ft)	P_s^+ (psi)	P^- (psi)	t_+ (msec)	t_- (msec)	Main Shock Time of Arrival (msec)	Second Shock Time of Arrival (msec)
1	1-Bow	447	--*	--	--	--	--	--
1	2-Stern	447	--	--	--	--	--	--
2	1-Bow	447	--	--	--	--	--	--
2	2-Stern	447	--	--	--	--	--	--
3	1-Bow	202	--	--	27.0	30.0	100.0	156.0
3	2-Stern	202	2.0	0.9	24.0	31.0	107.5	164.0
4	1-Bow	202	2.2	0.8	25.0	29.0	110.5	166.5
4	2-Stern	202	2.1	0.9	24.5	31.0	110.5	165.5
5	1-Bow	147	4.2	1.2	23.9	26.3	58.5	108.0
5	2-Stern	147	4.3	1.3	21.1	28.2	58.5	108.0

*Blank entry indicates no data acquired.

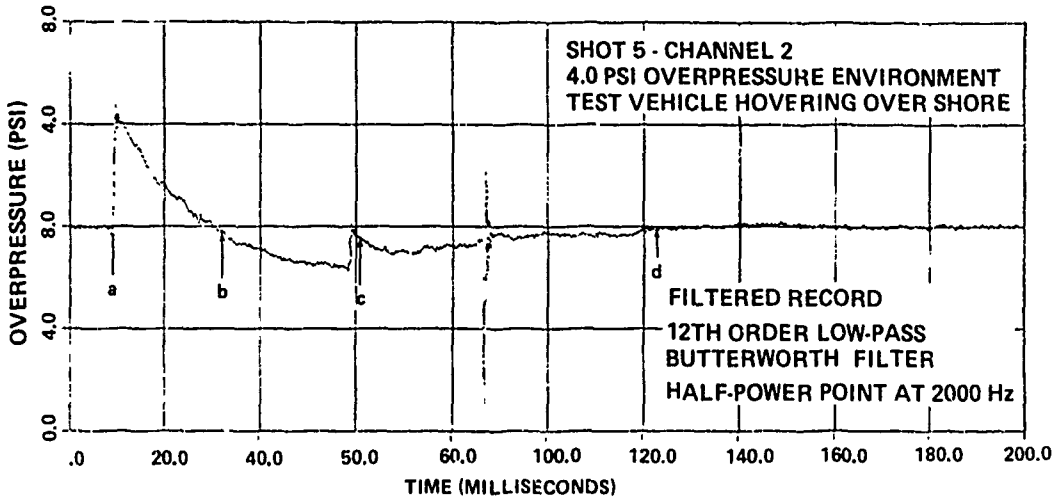

FIG. 8 FREE FIELD AIRBLAST PRESSURE HISTORY - SHOT 5, CHANNEL 2

(arrow d) is taken to be 115 msec. This total real loading duration is indicated on the shipboard airblast records to be discussed in the next section. Arrows b and c indicate the positions of the average time for the crossover from positive to negative phase and second shock arrival, respectively.

The "pressure spike" at the 87 msec location in Figure 8 is signal noise (dropout) and does not represent a true pressure measurement; the same "event" is also observed in the pressure record for the starboard, bow, and top shipboard gage locations. Intermittant noise of this character is observed to occur before and after shock arrival and is many times simultaneously recorded at several gage locations.

4.2 Shipboard Airblast Measurements and Calculated Load Functions

Representative shipboard airblast records are presented in Figures 9 through 12. The figures for the starboard (Figures 9(a), 10(a)) and port (Figures 9(b), 10(b)) sides contain plots of the corresponding load functions. The figures indicate a very poor correlation between the calculated profiles for airblast loading and the airblast data records. Arrows have been added to the airblast records to mark the following events.

Arrow Designations

s - Shock arrival at starboard gage

a - Shock arrival at gage location

b - End of positive phase (load function)

c - Second shock arrival (load function)

d - End of negative phase for 4 psi overpressure environment only (experimental value taken from Figure 8)

Calculated and measured values for peak reflected overpressure are compared in Table 5 for all shots. Free field overpressure measurements are included in the table for reference. The measured values of peak reflected overpressure for Shots 3 and 4 are greater than that calculated, which is not as expected.* During the test, the tethered vehicle could not be controlled sufficiently under wind loading** to

*The response of the airblast gage used aboard the test vehicle was not adequate for this application. For example, local acceleration peaks of 400 g's experienced in the 4 psi overpressure environment as measured by the translation accelerometer can significantly affect the response of the airblast gage. The longitudinal axis acceleration sensitivity for the airblast gage is 0.013 psi/g which can result in "5.2 psi pressure components" if 400 g local accelerations are experienced by the gage.

**Pressure components from wind loading are negligible; q_{WIND} = 0.5 psf for 20 ft/sec wind speed.

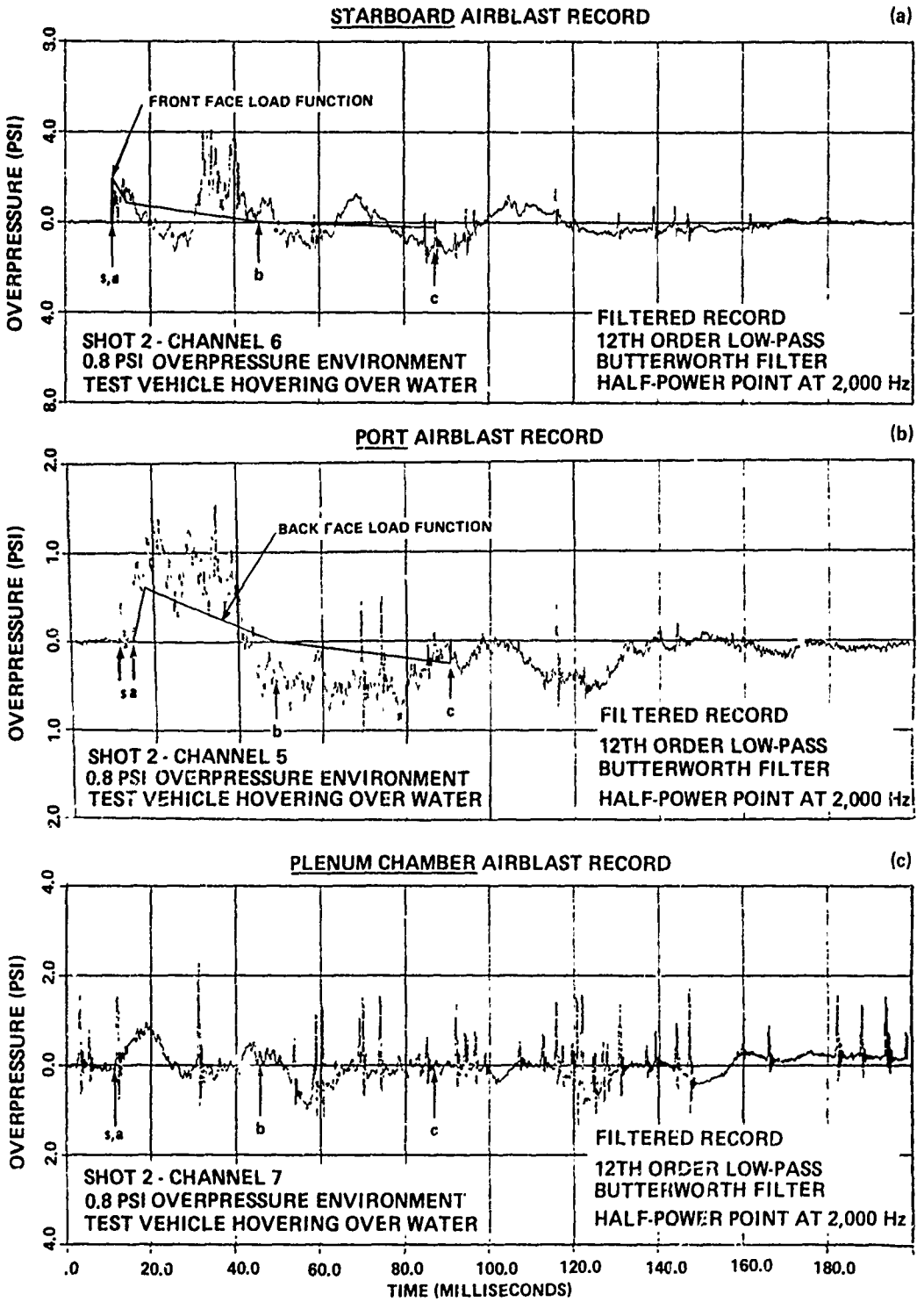

FIG. 9 SHIPBOARD AIRBLAST PRESSURE HISTORIES - SHOT 2, CHANNELS 5 - 7

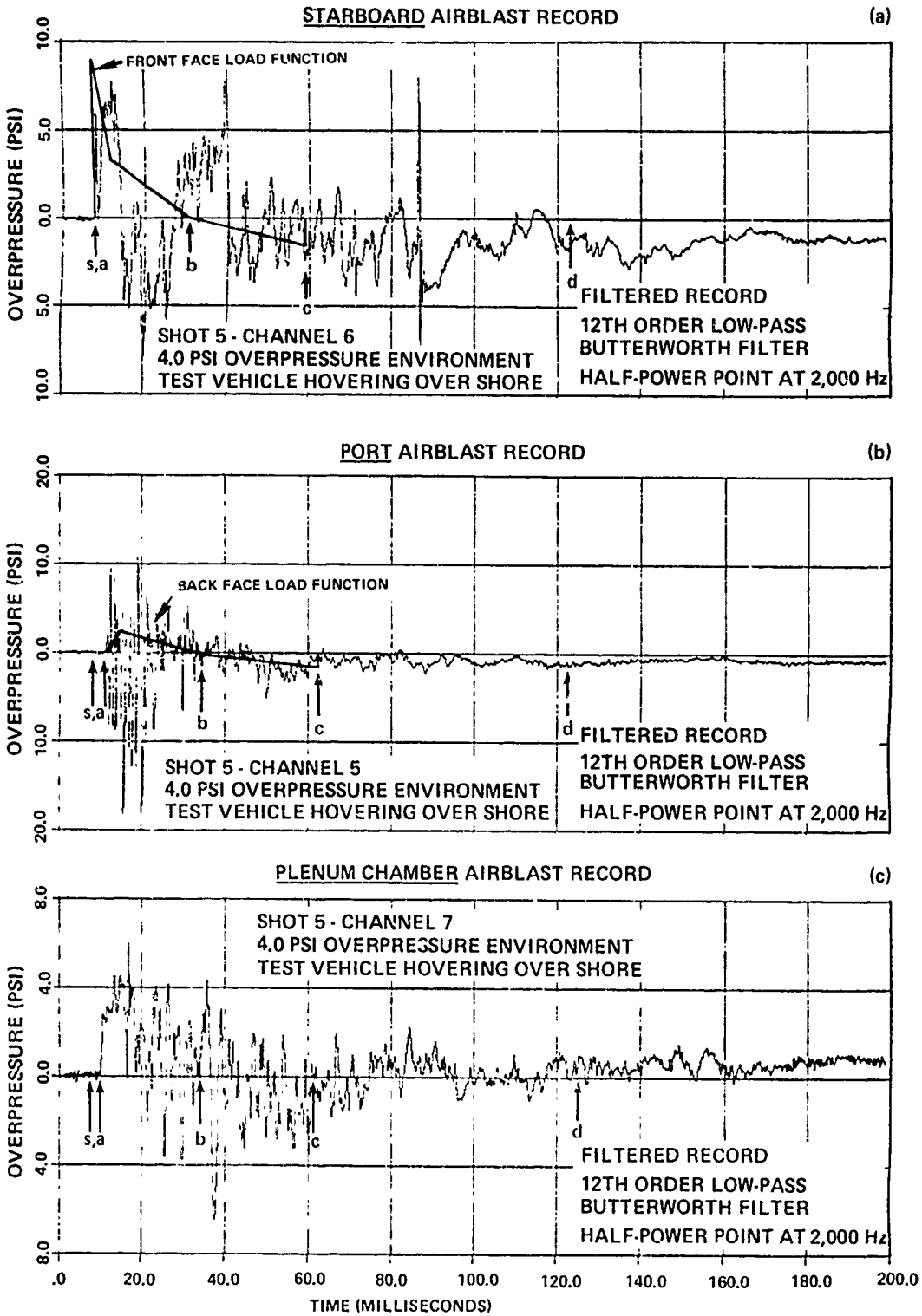

FIG. 10 SHIPBOARD AIRBLAST PRESSURE HISTORIES - SHOT 5, CHANNELS 5 - 7

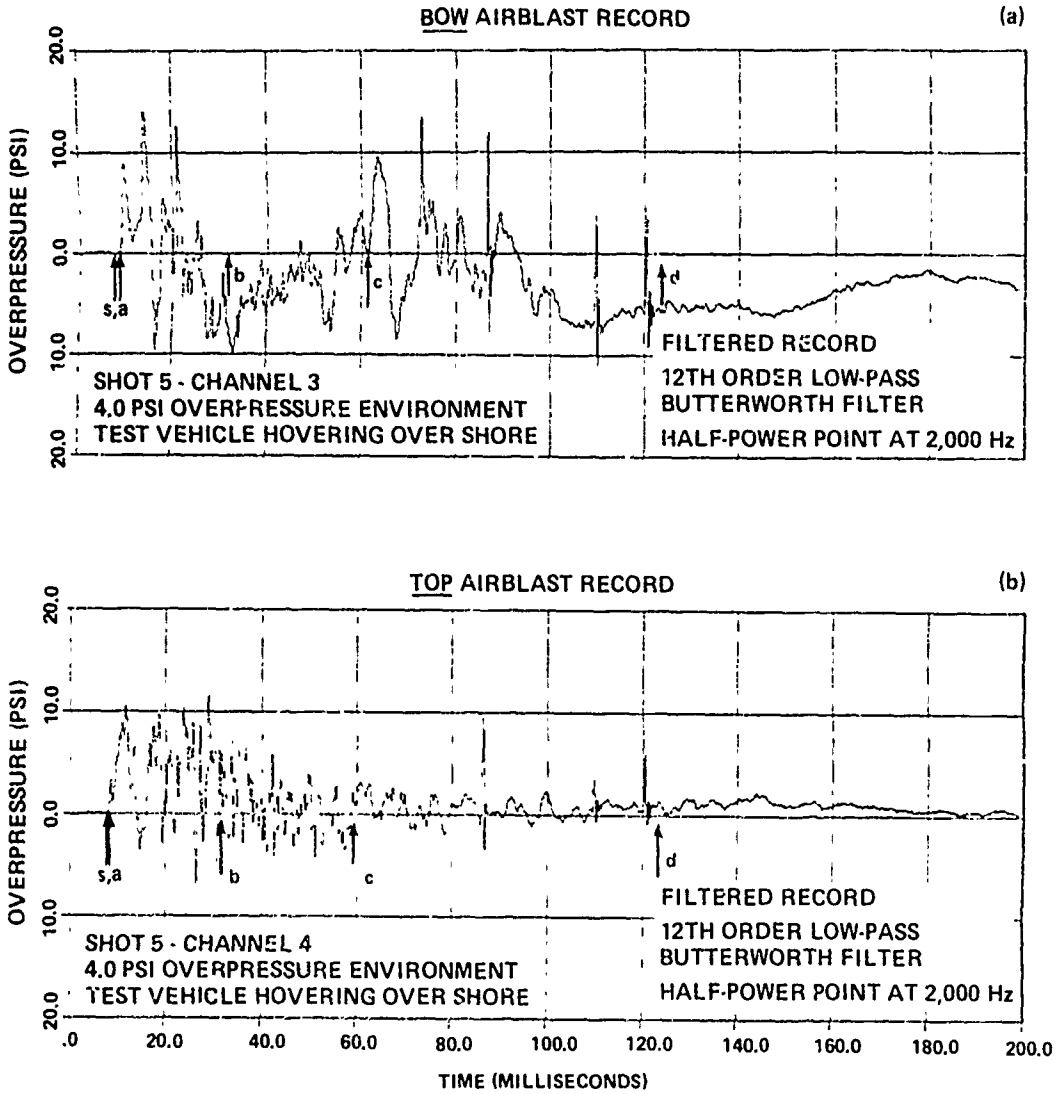

FIG. 11 SHIPBOARD AIRBLAST PRESSURE HISTORIES - SHOT 5, CHANNELS 3,4

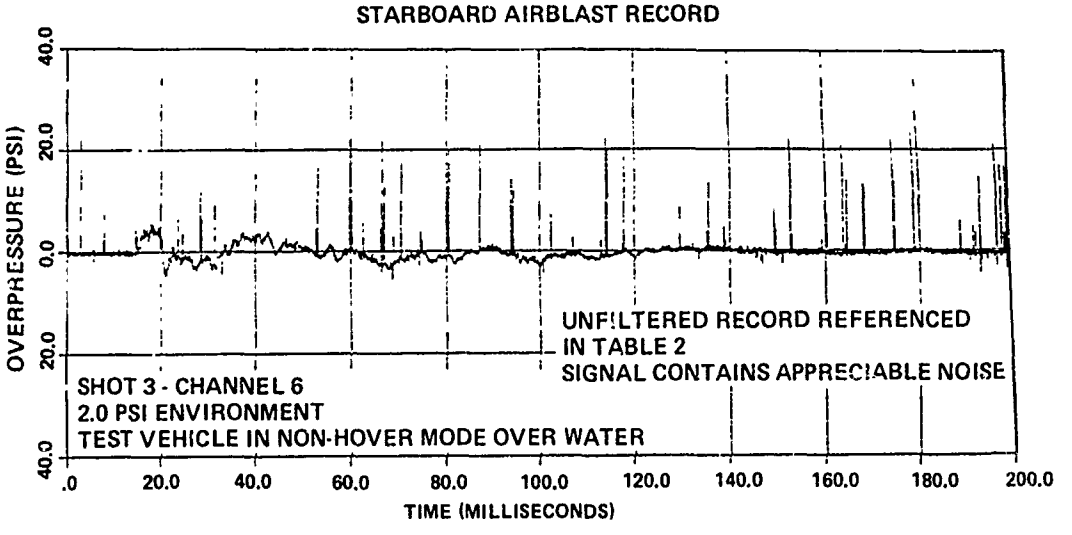

FIG. 12 EXAMPLE OF AN UNFILTERED SHIPBOARD AIRBLAST PRESSURE HISTORY - SHOT 3, CHANNEL 6

Table 5

COMPARISON BETWEEN CALCULATED AND MEASURED VALUES FOR FREE FIELD PEAK OVERPRESSURE AND PEAK REFLECTED OVERPRESSURE EXPERIENCED ON TEST VEHICLE BLAST SIDE

	Peak Free Field Overpressure (psi)		Peak Reflected Overpressure on Blast Side (psi)	
Shot	Calculated*	Measured (Avg.)	Calculated*	Measured
1	0.8	**	1.6	1.3
2	0.8	**	1.6	1.4
3	2.0	2.0	4.2	5
4	2.0	2.15	4.2	5.5
5	4.0	4.25	8.9	6.0

NOTES:

*Calculated overpressure is termed P_s^+ and calculated reflected overpressure is termed P_1 in Chapter 3. AIRBLAST RESPONSE MODEL of text

**No data acquired.

insure that the starboard side (the blast side) was aligned exactly normal to the blast direction. This being the case, it would be expected that the flow would not be completely stagnated at a blast side location, such as the starboard airblast gage position, thereby reducing the overpressure environment that would be experienced. For Shots 1, 2, and 5 the measured values for peak reflected overpressure are 20%, 15%, and 35% lower than the calculated values, respectively. KAPLAN, LEWIS, and MORRIS[4] presents an expression for calculating the peak reflected overpressure when the angle of incidence is taken into consideration. If the vehicle is oriented such that $\alpha = 35°$, the maximum angle of incidence applicable for the expression, the corrections are less than 3% for Shots 1 through 4, and 10 to 11% for Shot 5. A misalignment on the order of 35° was not observed in the data films and the correction for this effect does not account for the discrepancy reported above.

Figures 9 and 10 show that the airblast data records do not follow the load function profile for front face and back face blast loading. The starboard airblast records (Figures 9(a) and 10(a)) which correspond to blast side loading for Shot 2 (0.8 psi overpressure environment) and Shot 5(4.0 psi overpressure environment) contain several positive/negative phase components which are not indicated by the load function. However, the airblast gage is sensitive to applied accelerations and is undoubtedly responding to local acceleration loading experienced at the gage position on the test vehicle side panel. The port-side (lee side) airblast records (Figures 9(b) and 10(b)) follow the positive/negative phase duration of the ideal load function much more closely, although the profile amplitudes for the calculated loads and the data record do not agree.

The peak amplitudes for the plenum chamber airblast records for Shot 2 (Figure 9(c)) and Shot 5 (Figure 10(c)) correspond to the free field overpressure levels (measured relative to the plenum chamber levitation pressure).*

Airblast data records for the shipboard Bow and Top gage position are presented in Figure 11 for Shot 5 (4.0 psi overpressure environment).** In both cases peak overpressures greater than free

*Only a calculated value is available for the 0.8 psi overpressure environment (Shot 2).

**Some shipboard airblast gage measurements are observed to exhibit significant drift following the airblast loading. Gage response to the airblast thermal environment is a possible explanation for this behavior. The response of the airblast gage used in the present tests is similar to the thermal response of this gage discussed by SWISDAK.[7]

[7]SWISDAK, M. M., Jr., "Some Problems Associated with Airblast Transducers," presented at the Seventh Transducer Workshop, Telemetry Group, Commanders Council, Sandia Laboratories, Albuquerque, New Mexico, 4 through 6 April 1972, Minutes published and distributed by Secretariat, Range Commanders Council, White Sands Missile Range, New Mexico 88002.

field and even greater than reflected overpressure values are measured which suggests that the airblast gage is responding to local acceleration loads in addition to the applied overpressure. Also note that the port (lee side) airblast record (Figure 9(b)) registers a "pressure pulse" at the time of shock arrival at the starboard (blast side) gage location designated by arrow S.

The vehicle structure proved to be too flexible to allow reliable on-board pressure measurements. The operation of the shipboard airblast gages was greatly degraded by vehicle structural response in highly excited vibrational modes to the airblast loading.

4.3 Shipboard Acceleration Measurements and Calculated Vehicle Response

Translation and lift acceleration records for Shot 3 in which the test vehicle was in a 2.0 psi overpressure environment over water in a non-hover mode are given in Figure 13.* The acceleration measurements were taken at a mid-ship location in the vicinity of the test vehicle C.G. as described in Section 2.6.2 Acceleration Measurements. Indications of initial gage response for both accelerometers coincide within half-a-millisecond with the translation gage leading the lift gage.** The net horizontal loading which is used in the analytical model for the calculation of the test vehicle response to loading under airblast conditions for Shot 3 is included with the translation data record for reference. It should be pointed out that the theoretical load corresponds to a hovering vehicle without tether restraint, whereas the vehicle under test conditions for Shot 3 was in a tethered nonhovering configuration. Acceleration records for Shot 3 are the only unclipped acceleration data available from these tests; otherwise, acceleration data from Shot 2 or Shot 5 (test vehicle in hovering configuration) would have been discussed in place of Shot 3 data. Vibrational excitation of the vehicle structure produced by the airblast loading is indicated by the high frequency components in the acceleration record. The vibrational response is a "local" phenomenon and is not included in the airblast response model which is formulated to calculate rigid body response for the entire vehicle. However, the vibrational response of the vehicle is important. Signal clipping occurs with the high-amplitude, high-

*The translation and lift accelerometers which were mounted on the test vehicle measure acceleration components in body coordinates, not fixed laboratory coordinates. No correction is made for this in the results to be discussed since only small angular vehicle displacements under airblast loading were observed.

**The time scales for the two accelerometer records displayed in Figure 13 are somewhat misleading. The on-line electrostatic printer/plotter used for the data graphs in this report does not repeatedly reproduce the exact scale factor in the paper feed direction which in this case is the time axis. Also note that the arrival of the airshock at the starboard airblast gage location (blast side) is indicated in Figure 13 by the arrow "S".

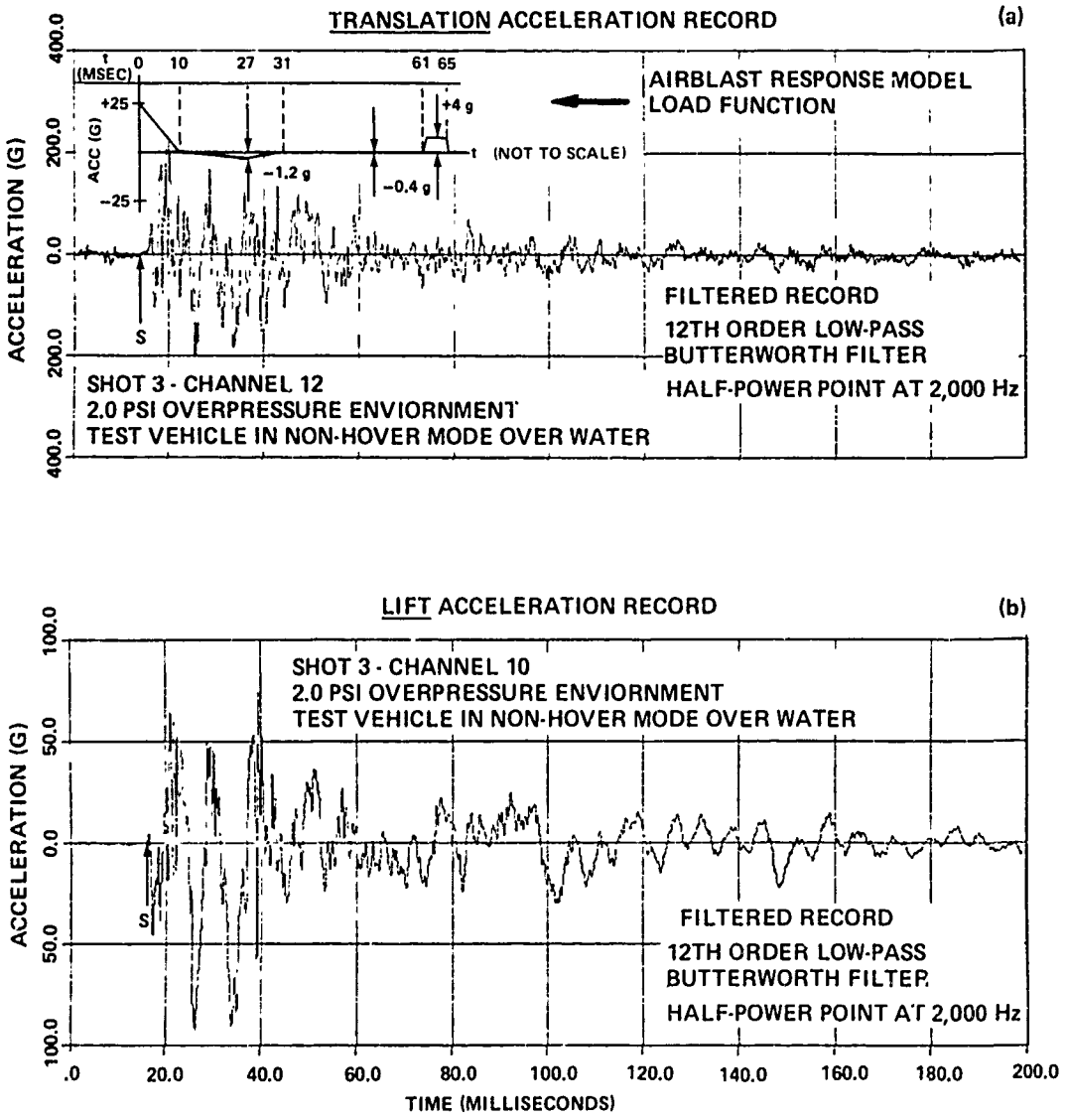

FIG. 13 SHIPBOARD ACCELERATION HISTORIES - SHOT 3, CHANNELS 10, 12

frequency peaks present in the acceleration data for Shots 4 and 5 which renders the records useless for calculating velocity and displacement responses to the airblast loading.

The velocity and translation integrals corresponding to the translation accelerometer record for Shot 3 are shown in Figure 14. The integration procedure "averages-out" the "local" contribution to the vehicle response as can be seen by comparing the acceleration record with the velocity and then with the displacement integrals. The results in Figure 14 are only qualitatively correct because of questionable signal amplitude scaling produced by incorrect conversion of tape recorder playback electronics during data digitization (see Section 4. DISCUSSION OF RESULTS in the text). Details on how the velocity and translation integrals were calculated are given in Appendix B.

The calculated rigid body response of the test vehicle in the 2.0 psi overpressure environment using the airblast response model acceleration loading (presented as . insert in Figure 13(a)) does not agree with the results obtained by integrating the acceleration data (compare solutions given in Figure 14).* An inspection of Figure 14 and the discussion in Appendix D indicate that the test vehicle tether system determined to a significant extent the vehicle response to the airblast loads. The final motion of the test vehicle as calculated from the acceleration data is directed towards ground zero in the negative blast direction. The airblast response model does not indicate this type of response even when underpressure loads are considered. The calculated loads in the negative blast direction, though they are applied throughout a major portion of the loading sequence, are not of sufficient magnitude to produce a reversal in the direction of vehicle motion.

The airblast response model does not consider forces in the lift direction in the present calculations. For Shot 3 in which the vehicle was in a non-hover mode over water airblast loads were applied over the upper surface of the test vehicle which were not balanced by airblast loads applied below the vehicle. The air cushion chamber below the vehicle within which an airshock/air-cushion interaction would have occurred had the vehicle been on-cushion was sealed by gravity at the water surface.

The response of the test vehicle to loading in the vertical direction for Shot 3 is given by the lift accelerometer record presented in Figure 13(b). Corresponding results for velocity and displacement response are given in Figure 15. As expected, the vehicle is shown to move downward. The velocity response in the lift direction, as does the velocity response for translation in the blast direction, contains "local" high amplitude vibrational responses to the airblast loading.

*Appendix C discusses the calculated rigid body response of the test vehicle subjected to the airblast model load functions. Appendix D discusses the calculated rigid body response of the test vehicle as determined from the acceleration measurements.

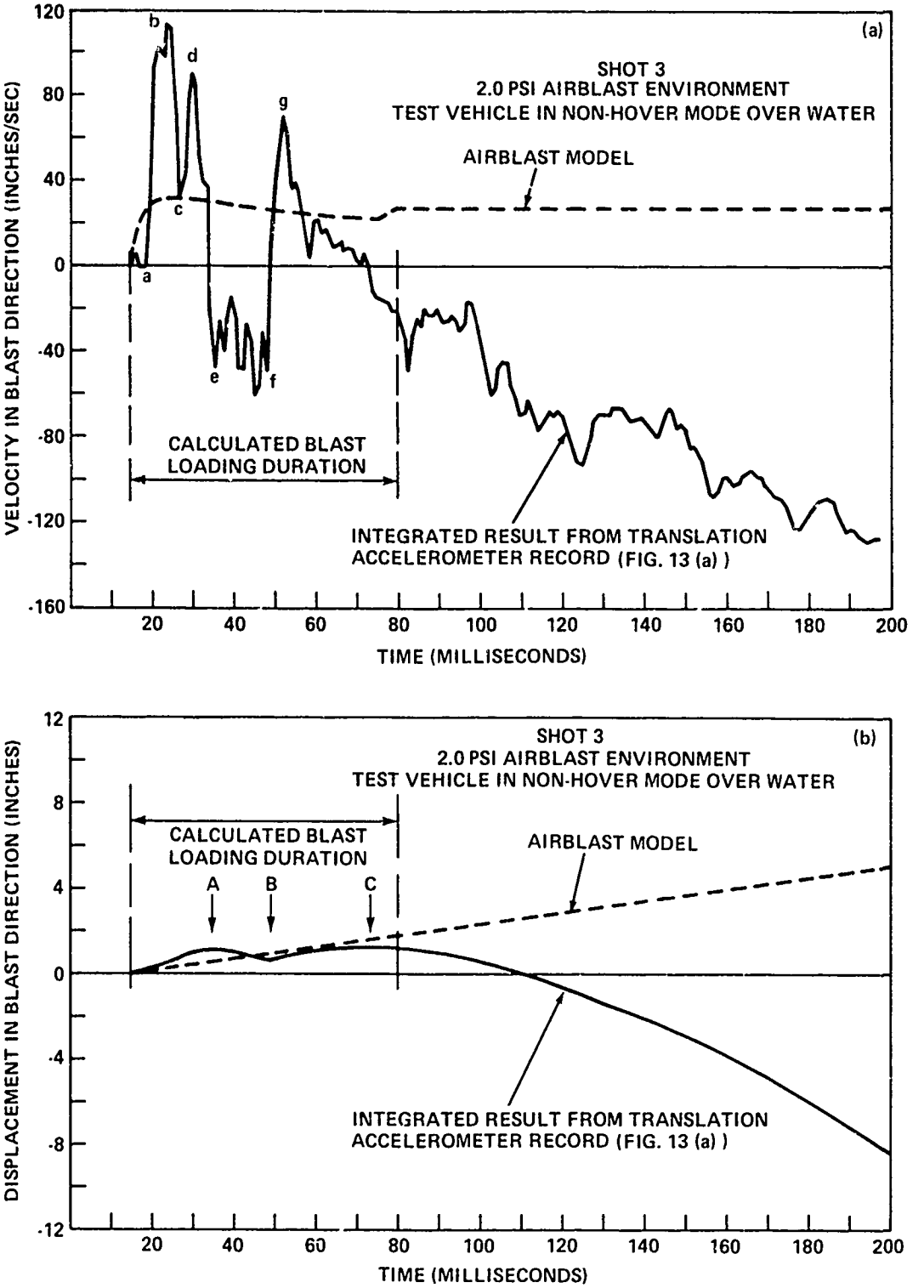

FIG. 14 TEST VEHICLE RESPONSE TO AIRBLAST LOADING - HORIZONTAL TRANSLATION

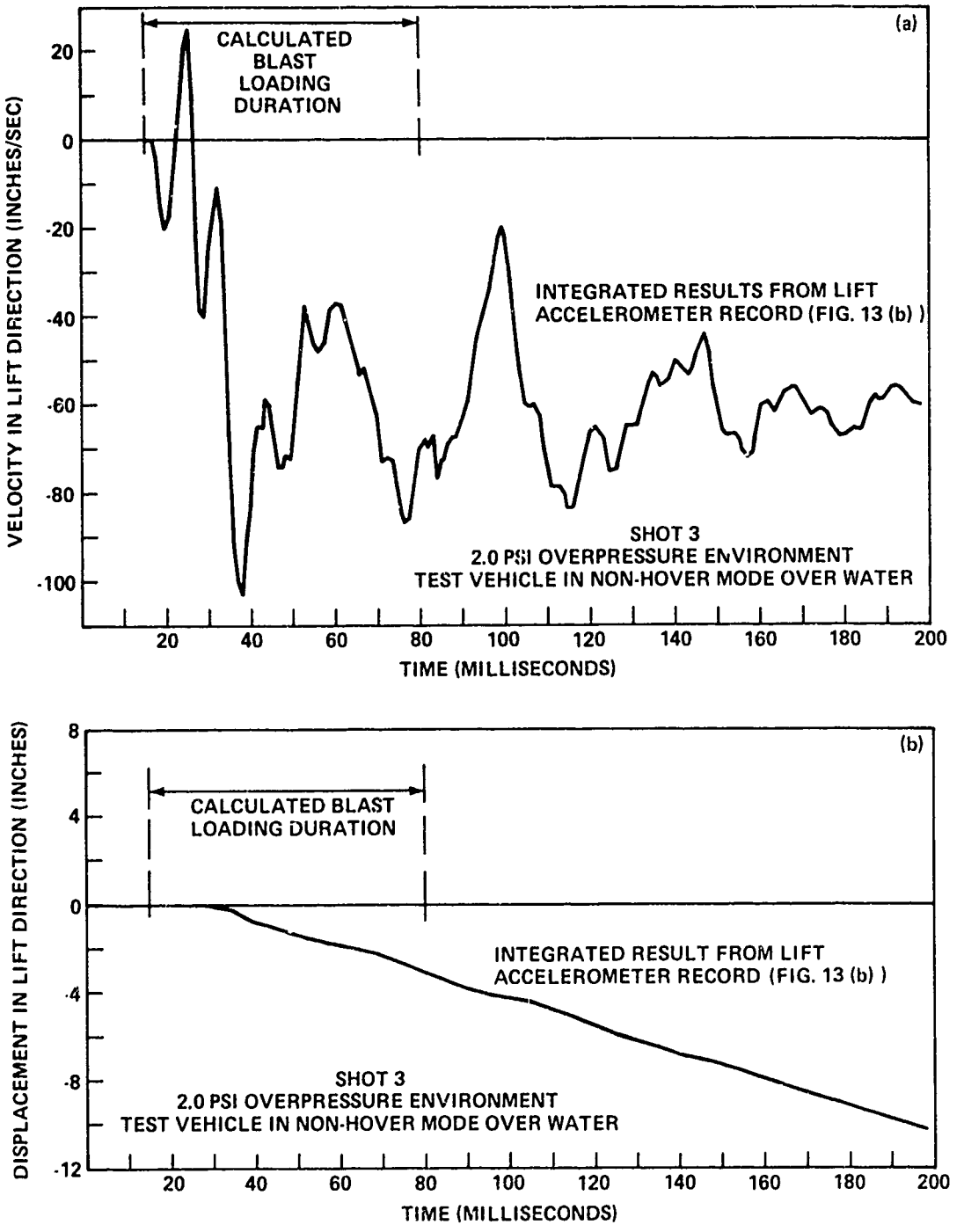

FIG. 15 TEST VEHICLE RESPONSE TO AIRBLAST LOADING - LIFT

Additional loads in the lift direction follow from buoyancy forces below the craft which oppose the airblast loading on the upper surface of the vehicle.

The data films do not confirm any vertical motion on the order of 10 to 12 inches as shown in Figure 15(b). Extrapolating the displacement results (or just extending the integration) for either the lift or the horizontal translation directions give vehicle displacements which are just not observed in the data films. This indicates that there is sufficient offset in the acceleration data signal within 200 msec of airblast loading to significantly affect the integrated results for velocity and displacement.

4.4 Photographic Coverage

There was not sufficient rigid body response of the test vehicle to the airblast loads to warrent detailed data film analysis. The films indicate that the vehicle did not move appreciably. During the tests there was a steady wind, determined to be ∿20 ft/sec for Shot 5, which positioned the test vehicle in an almost taut tethered condition downwind from the charge location. The tether did not permit significant vehicle translational response to the airblast loads for any of the five overpressure levels ranging from 1 psi to 4 psi since the loading proved to be insufficient to break the tether as planned.

Films for Shot 5, the 4.0 psi overpressure airblast environment with the vehicle hovering over shore, recorded structural damage to the test vehicle upon passage of the shock front. There was no structural damage to the vehicle for Shots 1 through 4.

The structural response observed for Shot 5 is best recorded on film HC14. The skirt on the lee side from the blast was ripped for almost the entire length of the vehicle and all the plastic lift fan blades were sheared off causing some damage to the plenum chamber duct. A discussion of the vehicle structural damage and a chronology of events for the Shot 5 airblast loading sequence is given in Appendix E.

5. SUMMARY OF RESULTS

The main objective for these tests was to determine the rigid body response of a small air cushion vehicle to an airblast environment. This was to be accomplished by conducting a series of free field, small scale tests with the vehicle exposed to the blast wave while hovering over water. The main test objective was not accomplished. No significant vehicle rigid body response to airblast loads was obtained. The test vehicle response was determined to be controlled by tether forces subsequent to and during airblast loading. Wind forces present at the test site controlled the test vehicle motion (when in a hovering condition) prior to airblast loading which suggests test vehicle vulnerability to airblast drag loading. The airblast impulse loads produced failures of the test vehicle lift fan blades and of the air cushion bag; the general method of these failures was determined. The test vehicle response to the airblast loading was filmed and onboard instrumentation was also included for measurements of pressure and acceleration. The data films indicate no significant response of the test vehicle to the airblast environment. However, vehicle structural damage in the 4.0 psi overpressure environment was recorded on film. The pressure and acceleration data were analyzed and compared with results calculated with the airblast response model developed. The pressure and acceleration records contain local acceleration components produced by vehicle vibrational response to the airblast loading. For this reason poor comparisons were obtained between data records acquired and airblast response model calculations. Improvements for instrumentation and test operation were determined.

6. RECOMMENDATIONS

The plastic shell structure of the test vehicle responded in highly excited vibrational modes to airblast loads of positive free field durations on the order of 25 to 35 msec. Structural stiffening members should be added to the vehicle if it is to be used in additional explosive tests. In particular, the vehicle structure needs to be strengthened and additional mass added at the gage mounting locations to dampen out vibrational response at these positions.

The test results indicate that the plastic lift fan blades and the nylon air cushion bag for this test vehicle cannot withstand airblast impulse loads (25 to 35 msec) corresponding to a 4.0 psi overpressure environment. The lift engine is shock mounted to the vehicle shell structure to reduce the transmission of engine vibration. Thus, the engine is not rigidly mounted to the fan duct. In response to the airblast loading, the lift engine moved with respect to the vehicle shell structure causing the fan blades to shear off when contact was made with the fan ducting. The air cushion bag, which runs along the lower periphery of the vehicle, ruptured under airblast loading; air was forced from the blast side portion of the bag to the lee side which then ripped after becoming over-inflated. The load level required to produce the above failures only pertains to the test vehicle; however, the method of failure applies to vehicles using similar designs for lift engine support systems and air bag construction.

Another vehicle tether system design is needed for any future free field explosive tests. Wind conditions at a test site require a fairly strong tether to maintain the vehicle position and orientation. Marlin line is adequate for this purpose. However, a much lighter tether is needed during the actual airblast loading. The tether should release the vehicle at an early stage in the airblast loading sequence to permit vehicle motion response to the loading. One way to satisfy these two opposing requirements is to tether the test vehicle with marlin line and then cut the tether during the firing sequence for charge detonation. With this method the vehicle position and orientation are maintained prior to firing but then the vehicle is untethered and free to respond to airblast loads following charge detonation. Of course, the vehicle is also free to respond to wind loading at this point. This response can be observed and accounted for during the time between charge detonation and shock arrival at the vehicle location.

Several improvements are recommended for shipboard measurements. As mentioned earlier, the airblast and acceleration gages should be mounted so as to reduce "local" acceleration components in the

measurements by strengthening the vehicle structure and increasing mass at the mounting location. The shipboard airblast gages used for these tests were found to be unsuitable for making pressure measurements onboard a craft of such flexible construction; the gages are too sensitive to the "local" high-amplitude, high-frequency acceleration components generated by the vehicle vibrational response to airblast loading. In addition to limiting the gage mounting structure vibrational response, acceleration-compensated airblast gages should be used for this application. Acceleration compensation can reduce the gage sensitivity to about 0.002 psi/g. The airblast records also indicate possibility of gage thermal response to the airblast environment. Better thermal response characteristics for this application can be obtained with quartz piezoelectric gages than with the lead zirconate titanate piezoelectric gages used in these tests; the respective thermal sensitivities are on the order of 0.01%/°F and 0.14%/°F. Improved acceleration measurements can be obtained using accelerometers with lower full-scale acceleration ranges. For example, the combined linearity and hysteresis for the translation accelerometer used in these tests is $\pm$0.75% of full scale output at zero acceleration which means that following airblast loading the accelerometer will return to zero acceleration (no load conditions) only within $\pm$0.75g since the full scale range for this gage is $\pm$100g's. A reduction in the instrument range to $\pm$10g is appropriate for these tests. However, to be able to use accelerometers with the reduced full scale range requires that the vehicle vibrational response to airblast loads be significantly damped as recommended above; otherwise, high-amplitude, high-frequency signal peaks, in response to vibrational excitation, will be clipped. It is also recommended that the gage recording equipment be mounted onboard so as to reduce gage cable length and to facilitate test vehicle motion response.

Determination of the test vehicle rigid body motion in response to airblast loading solely from acceleration data is difficult. The results and discussion in this report indicate the effects that signal drift and gage residual unbalance can have on the interpretation of the data. The data films for the present tests are used to set upper bounds on vehicle motion as calculated from the acceleration data and therefore help in determining the most appropriate way to handle the acceleration data.

The airblast response model should be extended to handle vehicle response in the vertical (lift) direction and should be applied to an SES. To accomplish this, airblast loads on the upper surface and below the vehicle (in passage through the air cushion) should be modeled. The NSRDC computer program TRANS, which was used for these calculations, can already consider forces due to gravity, buoyancy, air cushion pressure, and airblast forces acting on the upper surface of the vehicle; also SES sidewall hydrodynamic drag (in horizontal direction) is included whenever the sidewalls extend below the water surface. What is not included in this computer code at the present time is the interaction of the airshock with the air cushion and the contact of the vehicle with the water surface which restricts vehicle motion. The effects of the airblast negative phase loading are

included in the present model, but they do not appear to contribute to vehicle response in the horizontal (blast) direction. On the other hand, for vertical loading on the vehicle where larger loading areas are present and the possibility of airblast loading imbalance between the upper and lower vehicle surfaces exists, the contribution from underpressure loads may be significant and should be retained in the airblast response model.

To realistically check out an airblast response model, longer duration airblast loading test environments are required. A 1,000 pound (net explosive weight) charge is the largest charge size permitted for use at the test sites available for these experiments. The positive overpressure duration for a 1,000 pound charge terminates at 25 msec (7.5 airshock transient times across the vehicle) in the 2.0 psi overpressure regime. The loading duration is too short to produce appreciable vehicle response which can be separated from the vehicle response to steady local winds and to tether forces. It should be pointed out that the present airblast response model indicates an observable response to this level of loading because vehicle restraining forces are not included in the model. The net horizontal loading duration (in the positive blast direction) for the present test vehicle should be on the order of 75 msec ($\sim$20 airshock transit times) to simulate drag loading for future military vehicles (e.g., 2,000-ton SES) in a nuclear airblast environment (1 MT). Simulating the drag loading duration with respect to the airshock transit time across the vehicle is only one aspect of scaling the test vehicle experiment to a specific military vehicle design. Vehicle external profile (including rigid sidewalls), weight, moments of inertia, C.G./C.P. relative locations, and airblast overpressure to air cushion pressure ratio are some additional scaling parameters which need to be considered for modeling the rigid body response of an ACV/SES to airblast loading. Some compromises are necessary since not all scaling parameters can be satisfied simultaneously.

APPENDIX A: DATA FILTER

Figure A-1 displays an example of a free field airblast record. The top profile (a) is a plot of the digitized data as obtained from the original analog record; the sampling rate is 16,666/second. The next three profiles in descending order represent the airblast record after the application of a 12th order low-pass Butterworth digital filter (REED[A1]) with half-power points at (b) 2000 Hz, (c) 1000 Hz, and (d) 500 Hz, respectively. An inspection of Figure A-1 indicates how the data record is modified by use of a digital filter. The absolute time-of-arrival of the pulse is seen to increase as the half-power point frequency (the high frequency limit of the low pass filter) decreases.* This is because of the phase shift (produced by digital filtering) of the higher frequency components in the "fast-rise" or step portion of the airblast profile. Time measurements such as positive phase duration and relative arrival times for the first and second shocks are not appreciably affected, since they are determined by low frequency components where the phase shift is negligible. Also, the rise time of the step portion of the record is seen to increase as the high frequency limit of the low-pass filter decreases to 500 Hz.** A plot of the frequency response function and phase shift for the 12th order low-pass Butterworth Filter with a half-power point at 2000 Hz is provided in Figure A-2. This is the filter used with the airblast and acceleration data presented in this report. This particular filter is selected so as to attenuate the higher amplitude components of the signal dropouts without producing significant distortion to the signal dropout pulse widths. The higher frequency components correspond to vehicle structural response to airblast loading.

[A1] REED, R. S., "A Digital Computer Program for the Analysis of Wave-Form Data," Naval Ordnance Laboratory Report NOLTR 69-28, Jan 1969

*Zero time in Figure A-1 is arbitrary and does not correspond to time of detonation (Time Zero).

**A signal dropout occurs between 80 and 100 msec in Figure A-1 which can be edited out of the data record. This is not done here. Figure A-1 shows how the use of digital filtering distorts a signal dropout; the amplitude decreases and the pulse width increases as the high frequency limit of the low-pass filter decreases. A more reasonable representation of the data record in the vicinity of a signal dropout (if it can be determined that the "dropout" is not real information) is obtained by editing out the dropout. However, if a data record contains many dropouts, which is the case with some of the records here, the editing procedure can produce ambiguous results.

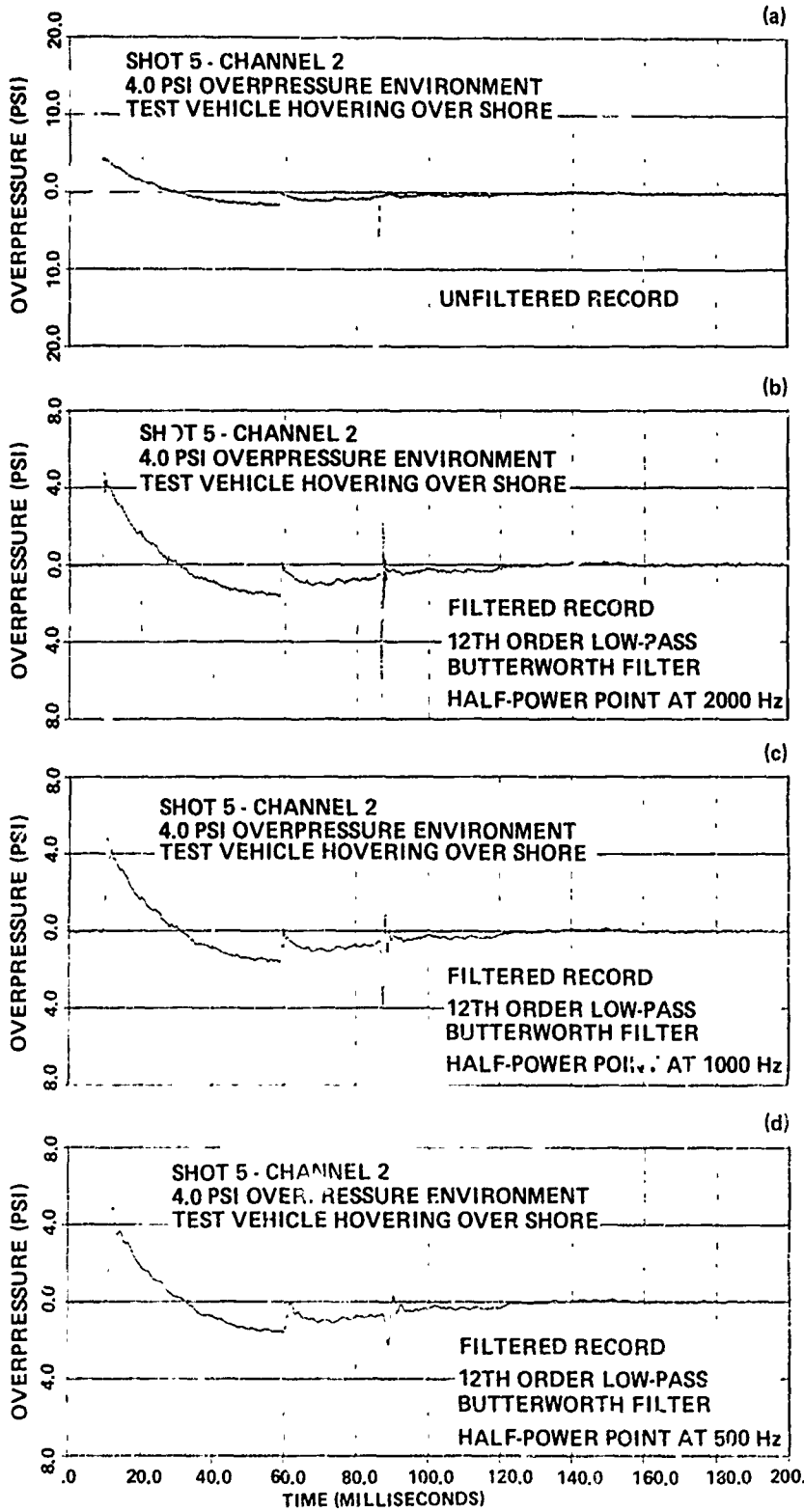

FIG. A–1 UNFILTERED AND FILTERED REPRESENTATIONS OF FREE FIELD AIRBLAST PRESSURE HISTORY - SHOT 5, CHANNEL 2

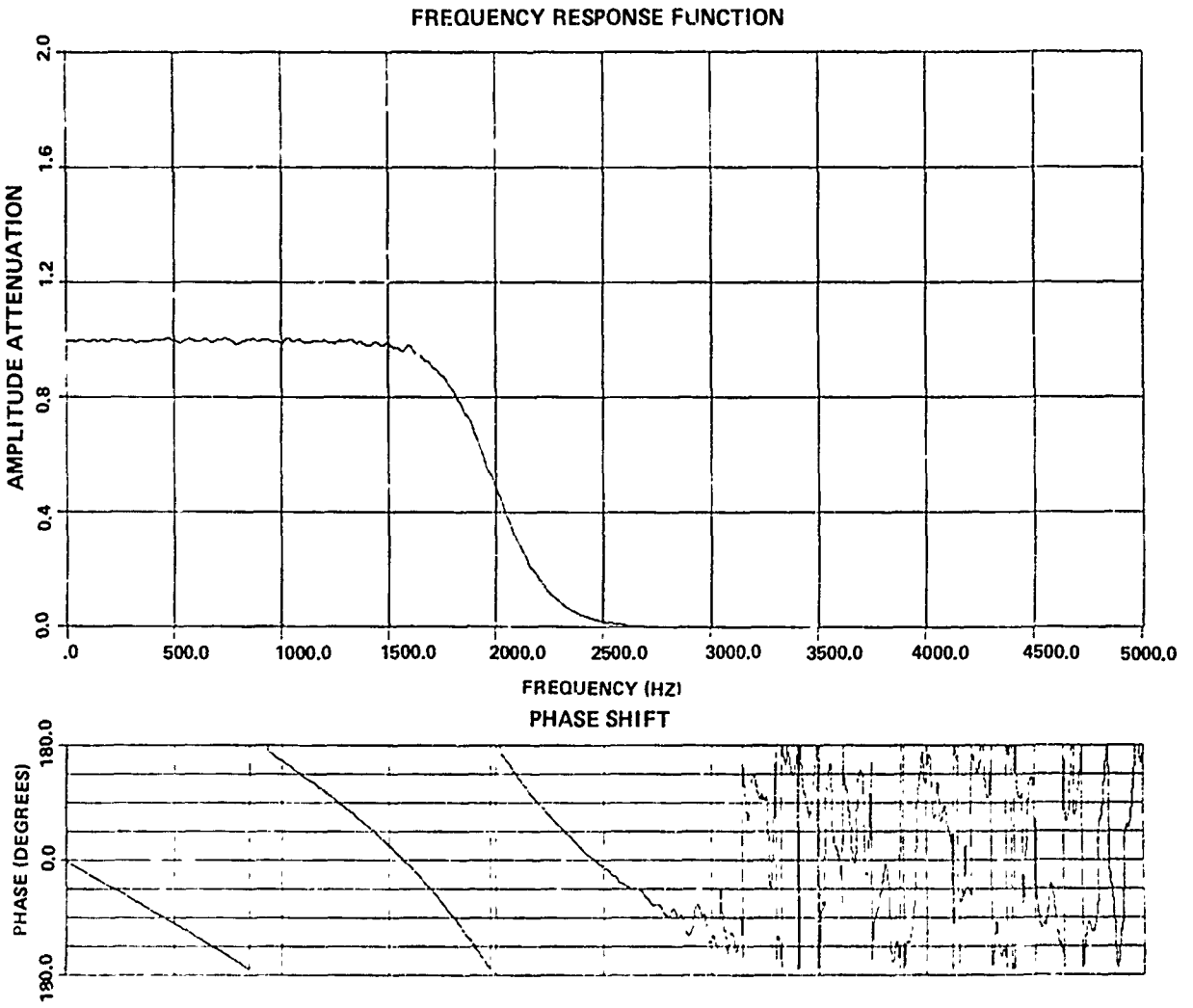

FIG. A–2 TRANSFER FUNCTION FOR 12TH ORDER LOW-PASS BUTTERWORTH FILTER WITH A HALF-POWER POINT AT 2,000 Hz

APPENDIX B: INTEGRATION OF ACCELERATION MEASUREMENTS

The integrated results for velocity and displacement are obtained using the computer code TRANS discussed briefly in Section 3.1 Response Model of text. A data baseline is established (in preparing the input for TRANS) by averaging the data signal for 55 msec prior to airblast arrival. The establishment of a data baseline normalizes or shifts the data.* There are several other methods available for handling the data; for the present data the above mentioned method appears to be the most appropriate since the forcing function (positive and negative phases of the blast loading) is of short duration (∿65 msec) and there is signal drift.

Another method for establishing the data baseline is to integrate the acceleration record over sufficient time for the vehicle motion to have ceased.** Then the data is normalized to insure that the value of the integral (which is equal to the final velocity) is zero. The critical step, for the present experimental results, with this method is in determining when vehicle motion has ended. Because the loading is of such short duration, integration of the acceleration record over sufficient time for motion to end (on the order of seconds) would require extensive modification to the data handling computer program and computer time costs would be high. Attempts were made to use this technique since accelerometer signals, in general, do not necessarily return to zero after loading; for example, the residual unbalance after loading for the translation accelerometer used for these tests can be up to ±5g which is a significant contribution when compared with the applied load as calculated by the airblast response model. Acceleration integrals are considered for 200 msec and 1 second durations following airblast arrival at the starboard gage location. In both cases the resultant displacement response is quite different from that shown in Figure 14(b). The final vehicle displacements after a 200 msec time period, calculated using the 200 msec and the 1 second acceleration integral modifications to the data, are +5 inches and +18 inches, respectively (not -8 inches, as shown in Figure 14(b)). But the data films for Shot 3 reveal no significant vehicle translational response to the airblast loading. A response of 18 inches is not observed; and, whether the vehicle moved five inches in the positive blast direction or eight inches in the opposite direction as indicated in Figure 14(b), cannot be determined from the data films. These displacements are too small to observe.

*This is the BASE data handling option in MRWSRD described by REED[B1].
**This is the MODIFY OFFSET data handling option in MRWSRD described by REED[B1].

[B1] REED, R. S., "A Digital Computer Program for the Analysis of Wave-Form Data," Naval Ordnance Laboratory Report NOLTR 69-28, Jan 1969

The acceleration integral modification to the data corresponding to the 200 msec duration should agree with the one second duration result if it is correct; the value of the acceleration integral for the longer duration would be the same as that for the short duration (providing that there is no appreciable signal drift) -- they should both be equal to the same final velocity if indeed the true final velocity has been reached. This is not the case here, so that the acceleration integral modification to the data corresponding to the 200 msec duration is not correct, even though the +5 inches value agrees very well with the air-blast model result indicated in Figure 14(b). For this reason, the base-line for the acceleration data is established using the data signal level for a short duration just prior to shock arrival; acceleration integral corrections are not applied.

APPENDIX C: AIRBLAST RESPONSE OF MODEL

The translational response of the test vehicle, as calculated by the airblast response model (represented by dashed lines in Figure 14(b)), is explained in the following manner.* The vehicle motion is in the positive blast direction (away from ground zero) since the blast side of the vehicle (starboard) is initially in a reflected overpressure environment. Then the reflected overpressure loading is reduced by rarefaction waves which originate around the vehicle side profile perimeter as the vehicle becomes engulfed in the airshock flow field. Following this clearing time ($t = t_2 =$ 3.8 msec) the reflected overpressure phase on the blast side gives way to the drag phase, the "steady" flow conditions (wind) associated with the airshock.

For this particular case the airshock transit time ($t = t_7 =$ 3.3 msec) across the vehicle is shorter than the duration of the unsteady diffraction phase (reflected overpressure phase) for the blast side. After the time for airshock transit, the overpressure loads begin to build up on the lee side of the vehicle. The flow on the lee side becomes steady after the interactions between the shock waves and rarefaction waves have subsided. The loads then correspond to the "steady" airshock wind conditions. This occurs at $t = t_8 =$ 6.8 msec. The force which this overpressure load exerts on the lee side of the vehicle is directed towards ground zero (in the negative blast direction) which tends to cancel the overpressure loads being applied on the blast side of the vehicle. The net horizontal load becomes directed in the negative blast direction at $t \cong 10$ msec. For this case, the dynamic pressure is negligible in comparison with the static overpressure for the flow conditions following the airshock. Because of this, the net horizontal force on the vehicle is in the negative blast direction (corresponding to approximately 1/2 to 1 g acceleration) for a portion of this time during airblast loading. This result occurs since the static overpressure behind the airshock is a decreasing function of particle time, and at a specific point in time during the "steady" airblast loading conditions the lee side of the vehicle is at an earlier particle time (hence, a higher static

*Refer to Section 3.2 Airblast Load Functions in the text for an explanation of terms used in connection with the loading functions. Refer to Figure 6 for the specific load functions used and to Figure 13(a) for the net horizontal load (airblast model) corresponding to overpressure levels in Shot 3. Subscripted time notation refers to Figure 6. Unsubscripted times refer to Figure 13(a) insert showing net horizontal load.

overpressure) than the blast side of the vehicle. There is not sufficient dynamic pressure on the blast side (and the lee side) in the airblast model to maintain a net horizontal load in the positive blast direction. For this reason the vehicle velocity (in the positive blast direction) begins to decrease in magnitude but does not decrease to zero so that the vehicle motion is still in the positive blast direction.

The positive overpressure phase of the airblast load is then followed by a negative phase during which the flow static pressure is below ambient pressure. On the blast side of the vehicle this occurs at $t = t_3 = 27.5$ msec. In the airblast model, the negative phase is terminated by the arrival of the second shock.* On the blast side of the vehicle this occurs at $t = t_4 = 60.5$ msec. The arrival of the negative phase and the second shock at the blast and then the lee side of the vehicle each differ in time by the duration of the transit time.

After the "steady" overpressure loading conditions for both the blast and lee sides if the vehicle, there is a period of time during which underpressure loads are applied on the blast side of the vehicle (loading in the negative blast direction) while overpressure loads are still being applied on the lee side of the vehicle. This is the time period $27.5 = t_3 < t < t_9 = 30.9$ msec. During this time there is a reduction in the net horizontal load (which is in the negative blast direction). This result follows because the overpressure load on the lee side of the vehicle decreases with time faster than the underpressure load on the blast side of the vehicle increases with time. The vehicle velocity (decreasing in magnitude) and displacement (increasing in magnitude) remain in the positive blast direction.

Following the above described transition period, underpressure loads are then applied to both blast and lee sides of the vehicle for a time. The underpressure loading increases in magnitude with increasing particle time behind the airshock until (in the airblast response model) the second shock arrives which terminates the loading function. During this loading phase, $30.8 = t_9 < t < t_4 = 60.5$ msec, the net horizontal force on the vehicle remains at a constant level, $\sim$1/2 g acceleration, in the negative blast direction. The vehicle velocity reduces in magnitude still further, yet remains in the positive blast direction as does the vehicle displacement.

The last phase of the airblast loading occurs when the second shock arrives at the blast side of the vehicle, $t = t_4 = 60.5$ msec. Then for the duration of the airshock transit time across the vehicle, $60.5 = t_4 < t < y_{10} = 63.8$ msec, the only loads applied to the

*The free field airblast record shown in Figure 8 indicates an additional underpressure phase (or negative phase) following the arrival of the second shock. This is not included in the airblast model.

vehicle in the airblast response model are the underpressure loads on the lee side. These loads are in the positive blast direction. The vehicle experiences a velocity increase in the blast direction and the vehicle continues to move in the same direction.

At the termination of the airblast loading the vehicle is in the following state.*

Final Values for Vehicle Velocity and Displacement Following Airblast Loading

2.0 psi Overpressure Environment (Calculation)

$x = 1.7$ inches

$V_x = 27.6$ inches/sec

$\theta = -0.6°$

$\dot{\theta} = -9.1°$/sec

There are no restraining forces in the airblast response model to account for the frictional resistance to vehicle motion or for tether forces. Because of this, the model predicts that the vehicle remains at a constant translational velocity in the blast direction and at a constant angular velocity after loading ceases.

Corresponding results for the 0.8 psi and the 4.0 psi overpressure environments using the loads defined in Figure 6 are listed below.

Final Values for Vehicle Velocity and Displacement Following Airblast Loading

0.8 psi Overpressure Environment (Calculation)

$x = 0.8$ inches

$V_x = 10.9$ inches/sec

$\theta = -0.3°$

$\dot{\theta} = -3.6°$/sec

*θ is defined in Figure 5. In the airblast response model, the rotational response of the vehicle is determined from the moment generated at the vehicle C.G. by the resultant pressure load applied at the vehicle C.P. If the C.P. and C.G. are aligned in the blast direction, there is no calculated rotational response to airblast loading. In this case the C.P. is located below the C.G.

4.0 psi Overpressure Environment (Calculation)

x = 3.4 inches

V_x = 64.0 inches/sec

Θ = 1.1°

$\dot{\Theta}$ = -21.0°/sec

APPENDIX D: AIRBLAST RESPONSE OF TEST VEHICLE DETERMINED FROM ACCELERATION MEASUREMENTS

The vehicle reversals-in-direction at positions A, B, and C (Figure 14(b)) as calculated from acceleration measurements for Shot 3 are not accounted for in the airblast response model. During the explosive tests the vehicle was tethered in the manner shown schematically in Figure D-1. Tethers 3 and 4 are near to being fully extended in the positive blast direction because there was a prevailing wind in that direction at the test site. The tethers, since they did not release the vehicle as planned, do limit the vehicle motion. From the relative positions of the vehicle C.G. and the blast side C.P., tether 3 becomes fully extended before tether 4 under airblast loading. This would account for the vehicle direction reversals indicated at points A (tether 3) and C (tether 4) in Figure 14(b). After the vehicle has moved in the negative blast direction (point B), tether force 3 is reduced to such an extent that the airblast loading once again forces the vehicle to move in the positive blast direction until the action of tether 4 (point C) becomes more dominant. Following this the airblast loading terminates. The vehicle then continues to move in the negative blast direction. This motion should continue until either tether 1 and/or tether 2 become fully extended or the vehicle motion is damped by drag forces.

It should be pointed out that the loads calculated by the airblast response model do not predict the vehicle response shown at point B in Figure 14(b). At this time the airblast response model indicates that the airblast loading is in the negative blast direction (and of small magnitude, $\sim$1/2 g acceleration) not the positive blast direction which is required to explain the vehicle reversal-in-direction at point B. The response at point B indicates that the airblast response model gives incorrect loads for this time period. The airblast loads must be in the positive blast location at this time.

The vehicle velocity response which is shown in Figure 14(a) contains several abrupt changes of large magnitude marked by symbols: a $\rightarrow$ b, c $\rightarrow$ d, d $\rightarrow$ e, and f $\rightarrow$ g. The sudden large velocity changes correspond to loads in the range of 50 to 80 g accelerations, and represent "local" vibrational responses (not vehicle rigid body responses) to airblast and tether loads. An inspection of the velocity record shows that caution should be used in the interpretation of the displacement record which has just been discussed. For example, the data records do show that the vehicle reverses directions at points A, B, and C (Figure 14(b)). What is called into question is the magnitude of the velocity and subsequently the displacement reversals. The presence of high amplitude vibrational responses to abrupt

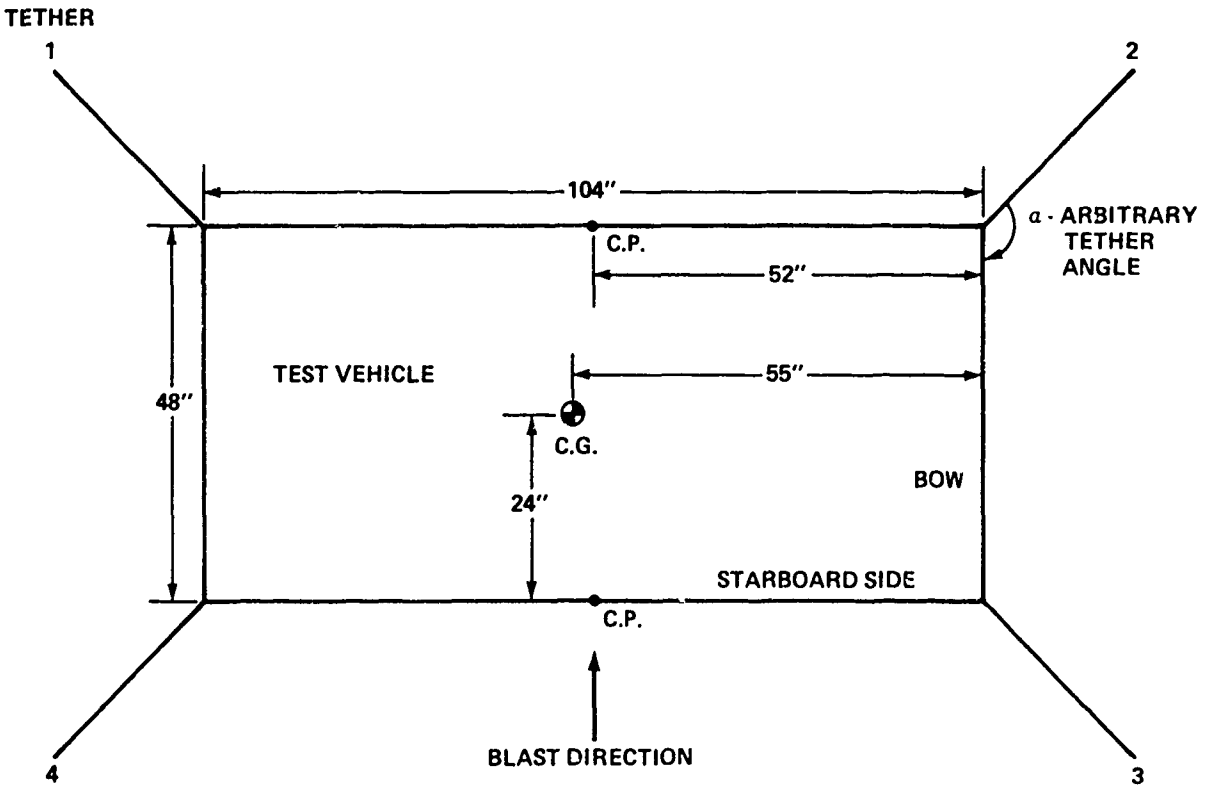

FIG. D–1 SCHEMATIC OF TEST VEHICLE TETHER SYSTEM

airblast and tether loadings can affect the magnitude of the vehicle response as calculated from the integration of the acceleration records.

APPENDIX E: OBSERVATIONS FROM DATA FILM HC14 FOR SHOT 5

Data film HC14 records the airblast response of the test vehicle for Shot 5, the 4.0 psi overpressure environment with the vehicle hovering over shore. This film provides the best coverage of the structural response of the vehicle and the sequence of events during airblast loading. Vehicle damage included loss of air cushion bag seal along vehicle lee side, loss of all plastic lift fan blades, and minor damage to the plenum chamber duct.

The air cushion skirt is in the form of a bag which follows the lower perimeter of the vehicle structure (see Figure 4). Upon arrival of the shock at the blast side of the vehicle, the portion of the bag running along this side of the vehicle, the blast side, is forced to collapse against the vehicle structure. The air originally filling the blast side portion of the air cushion bag is then directed into the lee side section which rips from being overinflated. The fan blade loss is probably due to the motion of the lift engine relative to the vehicle main structure and subsequent blade contact with the ductwork. The motion of the engine during the airblast response was such that the spark plug was also sheared off (determined from post-shot inspection) during the motion of the engine in the plenum chamber duct.

Film HC14 shows small flexural displacements on the blast-side and bow surfaces of the vehicle body. The vehicle is also shown to tilt downward towards the blast side; that is, looking towards the bow with the shock wave coming from the left, the vehicle rotates ($\sim$2 degrees maximum displacement) in a counterclockwise direction.

The initial rotational motion of the vehicle is produced by two major effects.

1. The centers of pressure (C.P.) for the side forces acting on the vehicle (blast side and lee side) are not aligned vertically with the vehicle G.G. The C.P. is below the C.G. for this test vehicle.

2. The portions of the shock passing above and below the hovering vehicle arrive at corresponding transverse locations on the vehicle at different times and with different shock strengths. The lower portion of the shock propagates below the vehicle into a confined region at a somewhat higher pressure (the air cushion pressure needs to be about 10 psf above ambient to support the vehicle), and there is a difference in flow paths between the upper and lower vehicle surfaces because of vehicle structural geometry.

The first effect described above provides vehicle rotational motion in the proper (observed) direction; the vehicle should tilt

down on the blast side since the C.P. is below the C.G. The second effect is not considered in the model for reasons discussed in Section 3.1 Response Model of the text. The initial rotational motion imparted by the second mechanism should be in the same direction as that produced by the first mechanism. The portion of the shock passing below the vehicle should require more time to become established and the propagation should lag that portion of the shock passing above the vehicle.

Yaw motion of the vehicle, which could have been caused by non-alignment of the C.P. on the blast side of the vehicle with the vehicle C.G. along the direction of blast propagation, is not observed in the data films.

The general sequence of events which was observed in data film HC14 is listed below.

t = 0 - Shock front is at the blast-side air-cushion skirt location of the test vehicle.

t = 10 msec - Air cushion skirt has collapsed against blast side of vehicle.

t = 12 msec - Lee side skirt rip damage is first observed.

t = 12 msec - Vehicle rotational motion is observed to begin.

t = 43 msec - Lift fan blade pieces first appear to emerge from duct.